TITLE:

Empirical fragility and vulnerability curves for buildings exposed to slow-moving landslides at medium and large scales

Authors:

Dario Peduto[a*], Settimio Ferlisi[a], Gianfranco Nicodemo[a], Diego Reale[b], Giovanni Pisciotta[c], Giovanni Gullà[d].

[a] Department of Civil Engineering, University of Salerno, Via Giovanni Paolo II, 132, 84084 - Fisciano (SA), e-mail: dpeduto@unisa.it; sferlisi@unisa.it; gnicodemo@unisa.it.

[b] Institute for Electromagnetic Sensing of the Environment (IREA – CNR), Via Diocleziano 328, 80124 Naples, Italy, e-mail: reale.d@irea.cnr.it.

[c] Via Ventaglieri, 77, 80135 Naples, Italy, e-mail: ing.gpisciotta@gmail.com.

[d] Research Institute for Geo-Hydrological Protection, National Research Council of Italy (IRPI – CNR), Via Cavour 4/6, 87036, Rende (CS), Italy, e-mail: giovanni.gulla@irpi.cnr.it.

Corresponding author:

[*]**Dario Peduto**
Department of Civil Engineering
University of Salerno
Via Giovanni Paolo II, 132, 84084 - Fisciano (SA)
e-mail: dpeduto@unisa.it, Tel. +39 089 964120; Mobile +39 3286935656

This is a post-peer-review, pre-copyedit version of an article published in **LANDSLIDES**. The final authenticated version is available online at: **http://dx.doi.org/10.1007/s10346-017-0826-7**

Abstract

Slow-moving landslides yearly induce huge economic losses worldwide in terms of damage to facilities and interruption of human activities. Within the landslide risk management framework, the consequence analysis is a key step entailing procedures mainly based on identifying and quantifying the exposed elements, defining an intensity criterion and assessing the expected losses. This paper presents a two-scale (medium and large) procedure for vulnerability assessment of buildings located in areas affected by slow-moving landslides. Their intensity derives from Differential Interferometric Synthetic Aperture Radar (DInSAR) satellite data analysis, which in the last decade proved to be capable of providing cost-effective long-term displacement archives. The analyses carried out on two study areas of southern Italy (one per each of the addressed scales) lead to the generation, as an absolute novelty, of both empirical fragility and vulnerability curves for buildings in slow-moving landslide-affected areas. These curves, once further validated, can be valuably used as tools for consequence forecasting purposes and, more in general, for planning the most suitable slow-moving landslide risk mitigation strategies.

Keywords: slow-moving landslides; DInSAR; building damage; fragility curves; vulnerability curves.

This is a post-peer-review, pre-copyedit version of an article published in **LANDSLIDES**. The final authenticated version is available online at: **http://dx.doi.org/10.1007/s10346-017-0826-7**

1. Introduction

Amongst natural hazards (UNEP 1997), landslides (slow-)moving on preexisting sliding surfaces – although rarely associated to loss of human life – can cause (even large) detrimental effects, from both social and economic points of view, mostly related to the attainment of serviceability/ultimate limit states in the exposed facilities, e.g. buildings and roads (Blochl and Braun 2005; Scavia and Castelli 2003). For this reason, in order to identify the most suitable risk mitigation strategies via structural and/or non-structural measures, scientific and technical communities are strongly interested in carrying out analyses aimed at estimating the expected consequences due to the reactivation/activation of the above types of landslides. In this regard, a deep knowledge on features of both slow-moving landslides (e.g. volume of the displacing mass, kinematics) and exposed facilities (stiffness/strength of constituting materials, state of maintenance, value) is required (Corominas et al. 2014). However, the collection of this relevant information is not an easy task due to the existence of several sources of uncertainties, in turn related to (Glade 2003): the peculiarities of factors that predispose/trigger a given slow-moving landslide; the spatial distribution of the intensity parameter and its temporal variability; the vulnerability value that might change from one facility to another even for similar slow-moving landslide intensity; the lack of comprehensive databases of damage to facilities and its increase (if any) over the time. The accessibility of the latter databases is of particular concern for consequence analysis purposes since most of the adopted procedures are empirically-based, provided that data on the intensity parameter associated with a given level of damage severity are available (Leone et al. 1996; Mansour et al., 2011). In this regard, referring to displacement patterns (and rates) experienced by a certain facility or set of facilities located in (or in the proximity of) slow-moving landslide-affected areas, useful information may derive by complementing the conventional monitoring techniques (i.e. inclinometers, GPS, topographic

This is a post-peer-review, pre-copyedit version of an article published in **LANDSLIDES**. The final authenticated version is available online at: **http://dx.doi.org/10.1007/s10346-017-0826-7**

leveling) with Synthetic Aperture Radar satellite data processed via Differential Interferometric (DInSAR) techniques (Cascini et al. 2013a; Ferlisi et al. 2015; Gullà et al. 2016; Peduto et al. 2016a, b). Several SAR archives are currently available spanning a long time interval of more than 20 years and ranging from the high resolution (i.e. the former generation ERS1-2, ENVISAT, RADARSAT1-2 and the current Sentinel-1 missions, all operating at C-band) to the very high resolution SAR sensors (i.e. COSMO-SkyMed, TerraSAR-X missions, both currently operating at X-band). The former group of sensors is more suitable for analyses over large areas, whereas the latter, thanks to the meter-scale resolution, is capable of following the displacement pattern over the time even of single detected facilities with sub-centimeter accuracy (Bianchini et al 2015; Nicodemo et al. 2016; Peduto et al. 2015, 2016c, 2016d, 2017). Focusing on buildings exposed to slow-moving landslide risk, this paper presents an original two-scale (1:25,000 – medium; 1:5,000 – large) procedure for vulnerability analysis, via both fragility and vulnerability curves, which is tested in two study areas of southern Italy. Values of the selected slow-moving landslide intensity parameters are derived from DInSAR data (Bianchini et al 2015; Catani et al. 2005; Cigna et al 2012; Lu et al. 2014) at either high- or very high-resolution; whereas the damage severity pertaining to the elements at risk (i.e. vulnerable areas including building aggregates at medium scale; single buildings at large scale) is estimated on the basis of information gathered from in-situ damage surveys.

2. Analysis of consequences to buildings at slow-moving landslide risk

Within the landslide risk analysis, the analysis of consequences to buildings due to slow-moving landslides is comprised of two sequential steps that, respectively, deal with the identification/quantification of the exposed buildings and the estimation of their vulnerability (Fell et al., 2008a). The former step involves detecting and classifying the buildings on the basis

This is a post-peer-review, pre-copyedit version of an article published in **LANDSLIDES**. The final authenticated version is available online at: **http://dx.doi.org/10.1007/s10346-017-0826-7**

of reliable information – to be collected via image processing and field surveys (Remondo et al. 2005; van Westen 2004) – concerning some relevant building characteristics (including the age of construction, structural and foundation typologies, occupancy type, number of floors). In analyses at medium scale, in order to overcome the difficulties associated with time consuming data collection and related inherent uncertainties (van Westen 2004; Pisciotta 2008), the use of aggregated levels (e.g. groups of buildings characterized by relative homogeneity of structural type) is recommended; whereas, single buildings can be accounted for in analyses at large scale (Cascini et al. 2008; Cascini et al. 2013a; Corominas et al. 2014; Maquaire et al. 2004; Palmisano et al. 2016; Peduto et al. 2016d; van Westen et al. 2008). Once the elements at risk are recognized and mapped by overlapping the slow-moving landslide-affected areas – provided by inventory maps – to territorial data, the same elements can be monetarily quantified (e.g. in terms of monetary value or replacement cost) (Amatruda et al. 2004; Blahut et al. 2014).

As far as the vulnerability of buildings is concerned, it can be conveniently defined – according to the scale of analysis – as "*the expected degree of loss to an aggregate of buildings (at medium scale) or to a single building (at large scale) due to the occurrence of a slow-moving landslide of a given intensity*". In both cases, the concept of "degree of loss" can be associated to the ratio of repair cost to monetary value/replacement cost that, in turn, relies on the (reversible or irreversible) damage induced to the exposed elements. This damage depends on both the landslide type mechanism and related intensity (i.e. differential displacements and/or their velocity whose spatial attributes result, for instance, from the position of the exposed elements with respect to the area affected by a slow-moving landslide) and the building characteristics (Fell et al. 2008b; Palmisano et al. 2016).

The vulnerability of buildings can be quantified using either vulnerability indices/curves or fragility curves. The vulnerability index expresses the expected degree of loss to a given

This is a post-peer-review, pre-copyedit version of an article published in **LANDSLIDES**. The final authenticated version is available online at: **http://dx.doi.org/10.1007/s10346-017-0826-7**

(aggregate of) building(s) on a numeric rating scale ranging from 0 (no loss) to 1 (total loss) (Corominas et al. 2014; Li et al. 2010; Uzielli et al. 2008). Vulnerability curves show the relationship between the mean level of damage severity to a given (aggregate of) building(s) and the value of the landslide intensity (adapted from Saeidi et al. 2009, 2012). Fragility curves provide the conditional probability for a given (aggregate of) building(s) of reaching or exceeding a certain level of damage severity as a function of the landslide intensity; thus they express the vulnerability of buildings in probabilistic terms, incorporating uncertainties (Mavrouli et al. 2014).

Based on the scale of the study area, the availability and quality of input data as well as the local construction technology, four main categories of fragility/vulnerability curves can be distinguished according to the adopted method (Negulescu and Foerster 2010; Mavrouli et al. 2014): heuristic, empirical, analytical and hybrid. Three main types of input data are necessary, namely (Saeidi et al. 2009): damage scale; building typology; intensity parameter. Up to now, few examples of fragility/vulnerability curves for buildings exposed to slow-moving landslides have been proposed in the scientific literature, mainly deriving from the adoption of analytical methods (Fotopoulou and Pitilakis 2013; Mavrouli et al. 2014; Pitilakis and Fotopoulou 2015).

3. The proposed methodology

The proposed two-scale procedure (Fig. 1) for the retrieval of empirical fragility/vulnerability curves for buildings exposed to slow-moving landslides includes: Phase I, in which the elements at risk are identified and classified according to the scale of analysis in a GIS environment; Phase II requiring the damage severity classification along with the selection of an intensity parameter; Phase III leading to the generation of fragility and vulnerability curves.

This is a post-peer-review, pre-copyedit version of an article published in **LANDSLIDES**. The final authenticated version is available online at: **http://dx.doi.org/10.1007/s10346-017-0826-7**

As far as Phase I is concerned, exposed aggregates of buildings are identified at 1:25,000 scale – on the basis of available base and thematic maps – according to the procedure extensively described in Cascini et al. (2013a) and appointed as "vulnerable areas" (Pisciotta 2008). In particular, considering that the urban fabric in small Italian towns selected for analysis purposes consists of adjacent buildings or terraced buildings rather than isolated buildings – mainly dating back from the late 19th to early 20th century – the identification of vulnerable areas involves the identification of similar buildings located on landslide-affected areas and "aggregated" according to their occupancy type and the structural typologies (i.e. masonry in the study area). At 1:5,000 scale, single buildings at risk (of either reinforced concrete or masonry) are identified by intersecting the information gathered from topographic maps with landslide inventory maps. In both scales of analysis, the value of elements at risk was not monetarily quantified being the estimation of slow-moving landslide risk beyond the scope of this paper.

In Phase II, the severity levels provided by Burland et al. (1977) and synthesized in Table I are adopted to classify the building damage recorded via in-situ surveys. In particular, at 1:25,000 scale these levels are roughly categorized in four classes (D0 = negligible, D1-D2 = from very slight to slight; D3 = moderate; D4-D5 = from severe to very severe) which mainly reflect the attainment of damages affecting the building aesthetics (D0 and D1-D2), causing a loss of functionality (D3) or even compromising the stability (D4-D5). Accordingly, the ad hoc predisposed fact-sheets to be filled during in-situ damage surveys at individual building level (Cascini et al. 2013a) do not involve gathering information on crack widths being this not relevant at 1:25,000 scale. Then, the equivalent damage (ED) severity level to be associated to a vulnerable area including at least one building whose damage severity exceeds the D0 class is established on the basis of the values taken by an equivalent damage index (f_k) and conservatively estimated by:

This is a post-peer-review, pre-copyedit version of an article published in **LANDSLIDES**. The final authenticated version is available online at: **http://dx.doi.org/10.1007/s10346-017-0826-7**

$$f_k = \frac{\sum_{j=0}^{3} c_j \cdot n_j}{n_{tot} - n_{D0}} \quad (1)$$

In Eq. (1), c_j is a numerical index conventionally associated to a *j*-class of damage severity (e.g. equally dividing the interval ranging from 0 to 5 into five sub-intervals and considering the higher break value pertaining to two merged levels, the following numerical indexes result: c_0 = 0 for D0; c_1 = 2 for D1-D2; c_2 = 3 for D3; c_3 = 5 for D4-D5); n_j is the number of buildings suffering the *j*-class of damage severity; n_{tot} is the total number of buildings included in the vulnerable area; n_{D0} is the number of buildings suffering the D0 class of damage severity. Accordingly, an ED severity level is labelled with *i)* ED1 if $2 \leq f_k < 2.5$, *ii)* ED2 if $2.5 \leq f_k < 3.5$, *iii)* ED3 if $3.5 \leq f_k \leq 5$; whereas ED0 indicates the ED severity level of a vulnerable area including only buildings whose damage severity is classified as D0. Another example of ED severity level assessment is provided by Antronico et al. (2014) but in their study the authors refer to weighted damage values for different portions of a given municipality.

At 1:5,000 scale, all levels of damage severity shown in Table I are considered to carry out in-situ damage surveys. In such a case, the ad-hoc predisposed fact-sheets (modified from Ferlisi et al. 2015) require to collect information about crack widths in order to distinguish clearly the structural pathologies pertaining to each of the exposed buildings.

The intensity parameter assumed at medium scale corresponds to the equivalent cumulative displacement (ECD) experienced by the vulnerable area in a given time interval coinciding with the period of observation of the available ERS1-2 satellite images. In particular, first the DInSAR benchmarks (i.e. the output measurement point of interferometric processing) whose velocity values can be projected from the satellite radar Line of Sight (i.e. LOS, which is typically tilted of some tens of degrees with respect to the vertical direction) to the steepest slope

This is a post-peer-review, pre-copyedit version of an article published in **LANDSLIDES**. The final authenticated version is available online at: **http://dx.doi.org/10.1007/s10346-017-0826-7**

direction (V_{slope}) are selected, according to the procedure described in Cascini et al. (2013a). Then, each building composing the aggregate is associated with a DInSAR-derived velocity value, which herein is indicated for sake of simplicity as building average velocity (V_{av_b}) and computed as the root mean square velocity via (Cascini et al. 2013a):

$$V_{av\_b} = \left(\sum_{i=1}^{N} \frac{w_{ci}}{w_{cN}} V_{slope\_i}^2 \right)^{1/2} \quad (2)$$

where

$$w_{cN} = \sum_{i=1}^{N} w_{ci}$$

$$w_{ci} = \frac{(1-\varepsilon_{\min})}{(C_{\max} - C_{\min})}(C_i - C_{\min}) + \varepsilon_{\min}$$

In Eq. (2), i refers to the i_{th} DInSAR benchmark on the building; N is the total number of DInSAR benchmarks on the building; $V_{slope\ i}$ is the velocity along the slope of i_{th} DInSAR benchmark. Moreover, weight values are established on the basis of the coherence parameter whose value quantifies the DInSAR measurement correlation over all the available acquisitions (the higher the coherence, the higher the weight value). Accordingly, w_{ci} is the coherence weight of the i_{th} DInSAR benchmarks on the building; C_i is the coherence value of the i_{th} DInSAR benchmark on the building; C_{max} is the maximum coherence value of the used dataset; C_{min} is the minimum coherence value of the used dataset; ε_{min} is a positive number not greater than 1 defining the weight of the DInSAR benchmark with the smallest coherence. In the analyses relevant to the dataset under investigation, ε_{min} value was empirically set to 0.2 thus assigning a weight of 20% to the smallest coherence value.

The cumulative displacement for each building derives from multiplying the estimated average velocity V_{av_b} for the period of observation. The ECD of the vulnerable area corresponds to the

This is a post-peer-review, pre-copyedit version of an article published in **LANDSLIDES**. The final authenticated version is available online at: **http://dx.doi.org/10.1007/s10346-017-0826-7**

average cumulative displacement, weighted on the number of DInSAR benchmarks covering each building composing the vulnerable area:

$$ECD = \frac{\sum_i \left(N_i \cdot D_{b,i}\right)}{\sum_i N_i} \quad (3)$$

where $D_{b,i}$ is the cumulative displacement associated to the i_{th} building within the vulnerable area and N_i is the ratio of the number of DInSAR benchmarks covering each building to the number of DInSAR benchmarks covering the whole vulnerable area.

At 1:5,000 scale, the intensity parameter is associated with the differential settlements (Δ) derived from the analysis of both high (i.e. ENVISAT) and very high-resolution (i.e. COSMO-SkyMed) DInSAR cumulative settlements for each exposed building (see also Bianchini et al. 2015; Peduto et al. 2017; Sanabria et al. 2014). In particular, the cumulative settlements are derived by multiplying the average velocity along the vertical direction (i.e. derived from the Line of Sight sensor-target direction) of each DInSAR benchmark covering a single building for the period of observation of the available dataset.

In Phase III (Fig. 1), by specializing the procedure proposed by several authors (Fotopoulou and Pitilakis 2013; Mavrouli et al. 2014; Negulescu and Foerster 2010; Negulescu et al., 2014; Peduto et al. 2016d, 2017; Saeidi et al. 2009, 2012), fragility curves are derived for both building aggregates composing the vulnerable areas (1:25,000 scale) and single buildings (1:5,000 scale) by combining the data on levels of equivalent damage or damage severity with the corresponding magnitudes of the specific intensity parameter (i.e. equivalent cumulative displacement at 1:25,000 scale or differential settlement at 1:5,000 scale). In particular, the probability of

This is a post-peer-review, pre-copyedit version of an article published in **LANDSLIDES**. The final authenticated version is available online at: **http://dx.doi.org/10.1007/s10346-017-0826-7**

reaching or exceeding a particular equivalent damage (*EDk*) or damage (*Di*) severity level for a fixed intensity parameter (*IP)* is respectively calculated as:

$$P\left(Equivalent\ Damage \geq EDk \middle| ECD\right) = \Phi\left[\frac{1}{\beta} ln\left(\frac{ECD}{\overline{ECD_l}}\right)\right] \qquad (k = 1, 2, 3) \tag{4}$$

or

$$P\left(Damage \geq Di \middle| \Delta\right) = \Phi\left[\frac{1}{\beta} ln\left(\frac{\Delta}{\overline{\Delta_l}}\right)\right] \qquad (i = 1, \ldots, 5) \tag{5}$$

where Φ[.] is the standard normal cumulative distribution function; $\overline{ECD_l}$ (or $\overline{\Delta_l}$) is the median value of the intensity parameter ECD (or Δ) at which the vulnerable area (or the building) reaches the equivalent damage (*k*) or the damage (*i*) severity level; and β is the standard deviation of the natural logarithm of the intensity parameter.

Finally, according to Lagomarsino and Giovinazzi (2006), vulnerability curves at medium and large scale are, respectively, derived by:

$$\mu_{ED} = a\,[b + tanh(c \cdot ECD + d)] \tag{6}$$

and

$$\mu_{D} = a\,[b + tanh(c \cdot \Delta + d)] \tag{7}$$

being μ_{ED} (or μ_D) the weighted average of the equivalent damage (or damage) severity levels for a given value of the intensity parameter ECD (or Δ); whereas a, b, c and d are four coefficients that must be determined for each scale of analysis.

This is a post-peer-review, pre-copyedit version of an article published in **LANDSLIDES**. The final authenticated version is available online at: **http://dx.doi.org/10.1007/s10346-017-0826-7**

4. Analysis at medium scale

4.1 Study area and available dataset

The study area (Fig. 2a), extending for about 557 km^2, includes 21 Municipalities of Benevento Province (Campania region, southern Italy). Base (i.e. topographic) maps at 1:5,000 scale and thematic (i.e. geological, geomorphological, landslide inventory) maps at 1:25,000 scale, developed by the National Basin Authority of "Liri-Garigliano and Volturno" rivers (NBA-LGV) within the Hydrogeological Setting Plans - Landslide Risk excerpt (HSP-LR) according to requirements of the Italian Law 365/2000, are available. The geological map of the study area highlights the existence of Mesozoic-Tertiary lithological units mainly consisting of clayey-sandy-arenaceous and clayey-calcareous-siliceous strata covered by marly-calcareous, arenaceous and arenaceous-conglomeratic units (Cascini et al. 2013a and citations therein). The latter units, together with the geo-structural setting, mainly control the geomorphological features of the area. As for the landslide inventory (Fig. 2a) a total of 2,180 slow-moving landslides (globally covering about 25% of the total extension of the study area) are mapped: 766 rotational slides; 267 rotational slide–earth flows; 1,117 earth flows; 30 deep seated gravitational slope deformations (DSGSD); moreover, 158 creep phenomena, 65 earth flow-creeps and 2 rotational slide-creeps are also inventoried (Cascini et al. 2013a; Calvello et al. 2016).

DInSAR displacement data used for the present study are provided by the nationwide Italian "Piano Straordinario di Telerilevamento" (MATTM 2010). They include 208 ERS images on ascending orbit (period September 1992 - September 2000) and 134 on descending orbit (period November 1992 - December 2000) processed by Persistent Scatterers Interferometry (PSI) algorithms (Costantini et al. 2008; Ferretti et al. 2001). By implementing the procedure described in section 3 (see also Cascini et al., 2013a) the projectable persistent scatterers (PS) were

This is a post-peer-review, pre-copyedit version of an article published in **LANDSLIDES**. The final authenticated version is available online at: **http://dx.doi.org/10.1007/s10346-017-0826-7**

selected (Fig. 2b) (7276 PS on ascending orbit and 7309 on descending orbit with an overall density of 26 PS/km^2).

The dataset of slow-moving landslide-induced damage to buildings includes information gathered from fact-sheets compiled during an extensive survey carried out in 2000 by technicians of NBA-LGV within the HSP-LR activities. The analysis of data revealed the presence of 95 buildings (all of masonry structural typology) experiencing damage whose severity ranges from D1-D2 to D4-D5 classes (Figs. 3a and 3b).

4.2 Results

In Phase I, a total number of 23 vulnerable areas including masonry building, for which both DInSAR data and the results of the damage survey are available, were identified. Out of 23 vulnerable areas 18 exhibited a damage severity exceeding the D0 class. An example of building aggregates characterized by homogeneity of structural (all masonry) and occupancy type is provided in Fig. 4a; whereas in Fig. 4b an example of the spatial distribution of vulnerable areas is shown.

Then, in Phase II, the f_k value was computed for each vulnerable area together with their ECD (i.e. the adopted slow-moving landslide intensity parameter). The percentage distribution of the obtained different levels of ED severity in the study area is shown in Fig. 5a; whereas Fig. 5b distinguishes the vulnerable areas with a given ED severity level according to the landslide type. An example of vulnerable areas with indication of both their ED severity level and ECD is shown in Figs. 5c and 5d referring to the municipality of Pesco Sannita.

By combining the above information, the relationship in Fig. 6a was derived. The diagram shows that the level of ED severity increases as the ECD (on average) increases.

This is a post-peer-review, pre-copyedit version of an article published in **LANDSLIDES**. The final authenticated version is available online at: **http://dx.doi.org/10.1007/s10346-017-0826-7**

Then, empirical fragility curves were derived for the vulnerable areas in the study area. To this aim, the frequency of occurrence of each ED severity level higher than ED0 (i.e. ED1, ED2 and ED3) was estimated for different DInSAR-derived ECDs (Fig. 6b). The probabilities of reaching or exceeding an EDk (k = 1, 2, 3) for given ECD values were computed by using Eq. (4) (Fig. 6c); the corresponding values of mean and standard deviation parameters are synthesized in Fig. 6c.

The work hypothesis of using the cumulative log-normal distribution to describe the probability of reaching or exceeding a given damage level was checked for the dataset at hand by using the Kolmogorov-Smirnov (K-S) goodness-of-fit test, as it is shown in the Appendix.

Finally, the vulnerability curve was derived for the study area by fitting the (μ_{ED}(ECD), ECD) data with the Eq. (6). In particular, for each of the ECD value obtained from the analysis of DInSAR data pertaining to the sample of vulnerable areas at hand (18), μ_{ED}(ECD) was computed with the obtained fragility curves according to the formula (adapted from Pitilakis and Fotopoulou 2015):

$$\mu_{ED}(ECD) = \sum_{k=1}^{3} P_k \cdot ed_k \tag{8}$$

where P_k is the discrete probability associated to an equivalent damage severity level (ED_k) whose numerical index equals ed_k (taken for this application as 1, 2 and 3 for ED1, ED2 and ED3, respectively).

The obtained vulnerability curve is shown in Fig. 6d and the corresponding fitting coefficients of Eq. (6) are: a = 295.6784; b = -0.9899; c = 0.2465; d = 2.6394.

This is a post-peer-review, pre-copyedit version of an article published in **LANDSLIDES**. The final authenticated version is available online at: **http://dx.doi.org/10.1007/s10346-017-0826-7**

5. Analysis at large scale

5.1 Study area and available dataset

The analysis at large scale refers to Lungro urban area (Fig. 7a) (Calabria region, southern Italy) located in a geological context where the Lungro-Verbicaro Unit, dating back to the Middle Trias and made up of metapelites and metacarbonates, prevails (Gullà et al. 2016). The inventory map of typified landslides (Fig. 7a), drawn-up according to the procedure given by Gullà et al. (2016), shows that several slow-moving landslides affect the study area. These phenomena can be distinguished in six typified categories (Table II) that from a kinematic point of view present the following characteristics: *i)* T_A1 landslides (slide-flow complex type) with ordinary velocity from 2 to 4 cm/year and critical velocity (i.e. in the paroxysmal phases) higher than 200 cm/year; *ii)* T_A2 landslides (slide-flow complex type) with ordinary velocity from 5 to 7 cm/year and critical velocity higher than 20 cm/year; *iii)* T_B1 landslides (slide-flow complex type) with ordinary velocity from 0.5 to 5 cm/year and critical velocity higher than 80 cm/year; *iv)* T_B2 landslides (slide-flow complex type) with ordinary velocity from 4 to 20 cm/year and critical velocity higher than 100 cm/year; *v)* T_C landslides (defined as landslide zone according to the definition provided in Antronico et al. 2014) with ordinary velocity from 0.5 to 5 cm/year and critical velocity higher than 40 cm/year; *vi)* T_D landslides (slide type) with ordinary velocity from 0.2 to 0.5 cm/year and critical velocity from 2 to 5 cm/year.

The analysis of historic data (1812 – 2011) indicates that for a long time Lungro historic centre has been severely affected by slow-moving landslides (Antronico et al. 2013, 2014; Gullà et al. 2016; Peduto et al. 2016a). Furthermore, a damage survey, carried out in October 2015 over the entire urban area, revealed that 111 buildings interact with the abovementioned landslides (Fig.

This is a post-peer-review, pre-copyedit version of an article published in **LANDSLIDES**. The final authenticated version is available online at: **http://dx.doi.org/10.1007/s10346-017-0826-7**

7a). In Figs. 7b and 7c the distribution of different levels of recorded damage severity is shown referring, respectively, to building typology and typified landslides.

The SAR image dataset used in this study was processed according to the SAR tomographic analysis (Fornaro et al. 2009, 2014), which is a recent extension of DInSAR processing framework particularly effective for single building monitoring with very high-resolution data (Cascini et al. 2013b; Peduto et al. 2015). It consists of 35 ENVISAT images acquired on ascending orbit (August 2003 to January 2010) as well as 39 COSMO-SkyMed images acquired on ascending orbit from October 2012 to April 2014. It is worth noting that the COSMO-SkyMed mission, composed by a constellation of four satellites, is currently one of the most advanced operational SAR system particularly effective for monitoring purposes of the built environment thanks to the very high spatial resolution of the acquired images as well as to the very fast acquisition scheduling of the multi-sensor mission. Figs. 8a and 8b show, respectively, the distribution of DInSAR benchmarks derived from ENVISAT (7299 DInSAR benchmarks) and COSMO-SkyMed data (15,252 DInSAR benchmarks). The significant coverage increase achieved by COSMO-SkyMed data and the highest velocity values recorded in both datasets in the central-eastern portion of the historic centre, mainly affected by T_D landslides, are also highlighted.

5.2 Results

For the purpose of the present study (Phase I), the analysis focused on 49 exposed buildings (12 of reinforced concrete and 37 of masonry structure) with shallow foundations and covered by at least two DInSAR benchmarks in both ENVISAT and COSMO-SkyMed datasets. Reinforced concrete buildings were built mostly after 1950s on a maximum of four floors. Masonry buildings, mainly made of disorganized stones (pebbles, or erratic/irregular stones), are low-rise

This is a post-peer-review, pre-copyedit version of an article published in **LANDSLIDES**. The final authenticated version is available online at: **http://dx.doi.org/10.1007/s10346-017-0826-7**

(2-3 floors) with ages ranging from about seventy to three hundreds years. The potential of DInSAR data in monitoring building settlements is shown in the example of Fig. 9 where, for a reinforced concrete building located on the boundary of an active roto-traslational slide, thanks to the availability of a dataset covering about 10 years, it is possible to follow the increase of the cumulative displacement also comparing it with the gradual increase of damage severity recorded during in-situ damage surveys.

Then in Phase II, differential settlements were computed for each building as the maximum difference of the cumulative settlements recorded by the DInSAR benchmarks within its perimeter (see Sect. 3) as shown in Fig. 10a. Moreover, for the period February 2010 - October 2012, when DInSAR data were lacking, a constant velocity value equal to the one associated to the longest available dataset (i.e. ENVISAT) was assumed. The merge of the above information with the results of the damage survey (Fig. 10b) allowed retrieving the relationship between differential settlements and the level of damage for both reinforced concrete (Fig. 10c) and masonry (Fig. 10d) buildings located on different typified landslides within Lungro area.

In Phase III, referring to masonry buildings suffering from damage severity levels spanning from D1 to D5 (29), the class frequency of occurrence (Fig. 11a) and empirical fragility curves (Fig. 11b) using the Eq. (5) were derived assuming the value of DInSAR-derived differential settlement as representative intensity parameter. The values of median and standard deviation parameters used to derive the fragility curves are synthesized in Fig. 11b. Similarly to the analysis carried out at medium scale, the reliability of the used cumulative log-normal distribution function was checked using the K-S test (see the Appendix).

Finally, the vulnerability curve was derived for masonry buildings of the study area by fitting the $(\mu_D(\Delta), \Delta)$ data with the Eq. (7), In particular, for each Δ value obtained from the analysis of DInSAR data pertaining to the sample of masonry buildings at hand (29), $\mu_D(\Delta)$ was computed

This is a post-peer-review, pre-copyedit version of an article published in **LANDSLIDES**. The final authenticated version is available online at: **http://dx.doi.org/10.1007/s10346-017-0826-7**

with the obtained fragility curves according to the formula (adapted from Pitilakis and Fotopoulou 2015):

$$\mu_D(\Delta) = \sum_{i=1}^{5} P_i \cdot d_i \quad (9)$$

where P_i is the discrete probability associated to a damage severity level (Di) whose numerical index equals d_i (taken for this application as 1, 2, 3, 4 and 5 for D1, D2, D3, D4 and D5, respectively). The obtained vulnerability curve is shown in Fig. 11c. The corresponding fitting coefficients of Eq. (7) are: a = 2.6745; b = 0.8695; c = 0.4810; d = -1.3310.

6. Discussion and conclusions

Although the potential of DInSAR data use in building damage assessment has been already addressed in the scientific literature (among the others, Arangio et al. 2013; Bianchini et al. 2015; Cascini et al. 2006, 2007, 2013b; Pratesi et al. 2015a, b; Peduto et al. 2016c, d, 2017; Sanabria et al. 2014) the proposed procedure for the analysis of building vulnerability to slow-moving landslides allowed for the first time the retrieval of empirical relationships between the level of equivalent damage (or damage) severity and the selected DInSAR-derived intensity parameters (i.e. equivalent cumulative displacement or differential settlement) at two different scales of analysis (medium and large) and for two different structural typologies (i.e. reinforced concrete and masonry buildings). The results highlight a general increasing trend of the above severity levels with slow-moving landslide intensity, independently from both the scale of analysis and the structural typology of the analyzed buildings. Moreover, the use of such a widespread information as DInSAR data also brought to the preliminary generation of empirical fragility and vulnerability curves for both masonry building aggregates in vulnerable areas (at medium scale) and single masonry buildings (at large scale). This could contribute to reduce the

This is a post-peer-review, pre-copyedit version of an article published in **LANDSLIDES**. The final authenticated version is available online at: **http://dx.doi.org/10.1007/s10346-017-0826-7**

lack of similar tools for this building typology in the field of slow-moving landslide consequence analysis. The applicability/exportability of the obtained results, although site-specific, could be significant if one considers that the majority of small villages in Italian southern Apennines exhibit similar urban fabric and structural typology as the ones considered in this study. In particular, widening the sample of analyzed buildings in similar geological-geomorphological contexts would allow calibrating and validating the generated curves. The generation of fragility/vulnerability curves for reinforced concrete buildings was hampered by their absence (at 1:25,000 scale) or their limited number (at 1:5,000 scale) within the sample of analyzed structures in the selected study areas. A test of the proposed methodology in urban areas where a sufficient number of DInSAR-covered slow-moving landslide-affected reinforced concrete buildings are present would allow generating similar empirical tools with the advantage, in this case, of making it possible a comparison with curves available in the scientific literature, mainly deriving from the adoption of analytical methods (Fotopoulou and Pitilakis 2013; Pitilakis and Fotopoulou 2015; Mavrouli et al. 2014).

As for the intensity parameters at the two different scales of analysis, the adoption of the equivalent cumulative displacements for vulnerable areas composed by building aggregates, which may not coincide with a single structure nor even contiguous ones, seems acceptable; on the other hand, the use of differential settlements for single buildings may require further deepening. In this regard, also other parameters – such as angular distorsion (Skempton and MacDonald 1956), deflection ratio (Burland 1995) and horizontal strain (Boscardin and Cording 1989) – should be considered, without neglecting the role of tilt (i.e. rigid body rotation) which a building might experience, in concurring to the attainment of serviceability/ultimate limit states. As for horizontal strain, where possible, the combination of DInSAR data on both ascending and descending orbits would allow the retrieval of the horizontal displacements that

This is a post-peer-review, pre-copyedit version of an article published in **LANDSLIDES**. The final authenticated version is available online at: **http://dx.doi.org/10.1007/s10346-017-0826-7**

could play a relevant role in building damaging (Boscardin and Cording 1989; Burland et al. 2004).

Furthermore, enlarging the dataset would allow further deepening concerning different factor presiding over damage occurrence such as, among others, the location of the building within the landslide-affected area (Corominas et al. 2014) and the foundation typology, so as to derive a more complete dataset of fragility/vulnerability curves. In particular, taking into account that for the present study the availability of DInSAR data acquired on a single orbit did not allowed to take into account the role played by horizontal displacement (condition that for landslide applications is common due to SAR acquisition geometry constraints), the construction of curves for defined structural typology and typified landslides (from both geo-mechanic and kinematic points of view), also taking into account the position of the building within the landslide-affected area, would allow analyzing/predicting building damage over portions of the phenomena where the ratio of horizontal to vertical component of the displacement vector can be assumed as constant. Accordingly, the horizontal component in those areas contributes in the same way to damage occurrence. As a result, disregarding the effects of horizontal displacements in a given portion of a typified landslide would homogeneously affect the results and, in turn, both their reliability and exportability.

However, since now it seems promising that the proposed procedure for the generation of empirical fragility/vulnerability curves may open new perspectives for helping authorities in charge of land use planning and/or urban management to select either most suitable zones to be urbanized or addressing restoration and adaptation policies. This result could be achieved at more affordable costs than the use of conventional monitoring techniques over wide number of exposed buildings.

This is a post-peer-review, pre-copyedit version of an article published in **LANDSLIDES**. The final authenticated version is available online at: **http://dx.doi.org/10.1007/s10346-017-0826-7**

Acknowledgements

The Authors are grateful to the National Basin Authority of Liri-Garigliano and Volturno (NBA-LGV) rivers and, in particular, to the General Secretary Dr. Vera Corbelli for providing all the thematic maps and the damage survey fact-sheets of the study area.

The Authors wish also to thank Italian Ministry of the Environment and Protection of Land and Sea and, in particular, Dr. Salvatore Costabile for providing the PSI data over NBA-LGV deriving from the "Piano Straordinario di Telerilevamento Ambientale".

The SAR image dataset used in the paper for the case study of Lungro was provided by European Space Agency (ESA) under the CAT-1 Project on "*Calibration of the Synthetic Aperture Radar (SAR) measures with Integrated Monitoring Networks (IMoN), and extended uses in homogeneous geological contexts*" (C1P.5618) and the Project carried out using COSMO-SkyMed® PRODUCTS, © ASI (Italian Space Agency), provided under license of ASI (prot. n. 0000155 dated 12 January 2015). The Lungro case study is part of the Project DTA.AD003.077.001 "Tipizzazione di eventi di dissesto idrogeologico" of the CNR Department of "Scienze del Sistema Terra e Tecnologie per l'Ambiente".

Appendix

This appendix is devoted to show the results of the Kolmogorov-Smirnov (K-S) goodness-of-fit test that was performed in order to check the work hypothesis of using the cumulative log-normal distribution for describing the probability of reaching/exceeding a given damage level within the fragility curve construction.

Fig. 12a shows the K-S test carried out on fragility curves derived for vulnerable areas composed by masonry building aggregates in the area analyzed at medium scale. The results confirm that the above work hypothesis is acceptable since the values of the maximum distances (D_{max}) between the considered log-normal distribution function for each damage level and the related empirical distribution function – defined according to the K-S test – are always lower than the critical values (D_{crit}) provided by Kolmogorov–Smirnov for all significance levels (α).

Similarly to the analysis carried out at medium scale, the reliability of the used cumulative log-normal distribution function was checked using the K-S test for the fragility curves derived for Lungro area. Also in such a case, the obtained results confirm the validity of the adopted work hypothesis (Fig. 12b).

This is a post-peer-review, pre-copyedit version of an article published in **LANDSLIDES**. The final authenticated version is available online at: **http://dx.doi.org/10.1007/s10346-017-0826-7**

References

Amatruda G, Bonnard Ch, Castelli M, Forlati F, Giacomelli L, Morelli M, Paro L, Piana F, Pirulli M, Polino R, Prat P, Ramasco M, Scavia C, Bellardone G, Campus S, Durville J-L, Poisel R, Preh A, Roth W, Tentschert EH (2004) A key approach: the IMIRILAND project method. In: Bonnard Ch, Forlati F, Scavia C (Eds.), Identification and mitigation of large landslide risks in Europe. Advances in risk assessment. A.A. Balkema Publishers, pp. 13-43.

Antronico L, Borrelli L, Coscarelli R, Gullà G (2014) Time evolution of landslide damages to buildings: the case study of Lungro (Calabria, southern Italy). Bull Eng Geol Environ, 74:47-59.

Antronico L, Borrelli L, Peduto D, Fornaro G, Gullà G, Paglia L, Zeni G (2013) Conventional and innovative techniques for the monitoring of displacements in landslide affected area. In: Margottini C., Canuti P, Sassa K (Eds.) Landslide science and practice – Early warning, instrumentation and monitoring. Springer-Verlag – Vol. 2, pp. 125-131.

Arangio S, Calò F, Di Mauro M, Bonano M, Marsella M, Manunta M (2013) An application of the SBAS-DInSAR technique for the assessment of structural damage in the city of Rome, in Structure and Infrastructure Engineering: Maintenance, Management, Life-Cycle Design and Performance, Vol. 10, pp. 1469-1483, http://dx.doi.org/10.1080/ 15732479.2013.833949.

Bianchini S, Pratesi F, Nolesini T, Casagli N (2015) Building deformation assessment by means of Persistent Scatterer Interferometry analysis on a landslide-affected Area: The Volterra (Italy) case study. Remote Sens, 7:4678- 4701, doi:10.3390/rs70404678.

Blahut J, Glade T, Sterlacchini S (2014) Debris flows risk analysis and direct loss estimation: the case study of Valtellina di Tirano, Italy. Journal of Mountain Science, 11(2), doi: 10.1007/s11629-013-2806-2.

Blochl B, Braun B (2005) Economic assessment of landslide risks in the Schwabian Alb, Germany - research framework and first results of homeowners and experts surveys. Nat Hazards Earth Syst Sci 5:389–396.

Boscardin MD, Cording EG (1989). Building response to excavation induced settlement. Journal of Geotechnical Engineering, 115:1-21.

Burland JB (1995) Assessment of risk of damage to buildings due to tunnelling and excavation. Invited Special Lecture, Proc of the 1st Int Conf on Earthquake Geotechnical Engineering, IS-Tokyo ‘95, pp. 1189-1201.

Burland JB, Broms BB, de Mello VFB (1977) Behaviour of foundations and structures. SOA Report, Proc of the 9th Int Conf on Soil Mechanics and Foundation Engineering, Tokyo – Vol. 2, pp. 495-546.

Burland JB, Mair RJ, Standing JR (2004) Ground performance and building response due to tunnelling, London. Proc of the Conference on Advances in Geotechnical Engineering, London, Thomas Telford Publisher – Vol. 1, pp. 291-342.

This is a post-peer-review, pre-copyedit version of an article published in **LANDSLIDES**. The final authenticated version is available online at: **http://dx.doi.org/10.1007/s10346-017-0826-7**

Calvello M, Peduto D, Arena L (2016). Combined use of statistical and DInSAR data analyses to define the state of activity of slow-moving landslides. Landslides, in press, doi: 10.1007/s10346-016-0722-6.

Cascini L, Ferlisi S, Fornaro G, Lanari R, Peduto D, Zeni G (2006). Subsidence monitoring in Sarno urban area via multitemporal DInSAR technique. International Journal of Remote Sensing Vol. 27, No. 8, 20 April 2006, 1709-1716. Taylor and Francis, ISSN 0143-1161, doi: 10.1080/01431160500296024.

Cascini L, Ferlisi S, Peduto D, Fornaro G, Manunta M (2007) Analysis of a subsidence phenomenon via DInSAR data and geotechnical criteria. Italian Geotechnical Journal, Vol. XLI (4):50-67, ISSN: 0557-1405.

Cascini L, Ferlisi S, Peduto D, Pisciotta G, Di Nocera S, Fornaro G (2008) Multitemporal DInSAR data and damages to facilities as indicators for the activity of slow-moving landslides. In: Chen Z, Zhang J, Li Z, Wu F, Ho K (Eds.), Landslides and Engineered Slopes. From the Past to the Future. Proc of the 10th Int Symp on Landslides and Engineered Slopes, 30 June-4July 2008, Xi'an (China), Taylor and Francis Group, London – Vol. II, pp. 1103-1109.

Cascini L, Peduto D, Pisciotta G, Arena L, Ferlisi S, Fornaro G (2013a) The combination of DInSAR and facility damage data for the updating of slow-moving landslide inventory maps at medium scale. Nat Hazards Earth Syst Sci, 13:1527-1549.

Cascini L, Peduto D, Reale D, Arena L, Ferlisi S, Fornaro G (2013b) Detection and monitoring of facilities exposed to subsidence phenomena via past and current generation SAR sensors. J Geophys Eng, 10 064001, doi:10.1088/1742-2132/10/6/064001.

Catani F, Casagli N, Ermini L, Righini G, Menduni G (2005) Landslide hazard and risk mapping at catchment scale in the Arno River basin. Landslides, 2:329–342.

Cigna F, Bianchini S, Casagli N (2012) How to assess landslide activity and intensity with Persistent Scatterer Interferometry (PSI): the PSI-based matrix approach. Landslides, 10:267–283.

Corominas J, van Westen C, Frattini P, Cascini L, Malet J-P, Fotopoulou S, Catani F, Van Den Eeckhaut M, Mavrouli O, Agliardi F, Pitilakis K, Winter MG, Pastor, Ferlisi S, Tofani V, Hervás J, Smith JT (2014) Recommendations for the quantitative analysis of landslide risk. Bull Eng Geol Environ, 73:209–263, doi: 10.1007/s10064-013-0538-8.

Costantini M, Falco S, Malvarosa F, Minati F (2008) A new method for identification and analysis of persistent scatterers in series of SAR images, IEEE International Geoscience & Remote Sensing Symposium, July 6-11, 2008, Boston - Massachusetts, USA, pp. 449–452.

Fell R, Corominas J, Bonnard C, Cascini L, Leroi E, Savage WZ on behalf of the JTC-1 Joint Technical Committee on Landslides and Engineered Slopes (2008a) Guidelines for landslide susceptibility, hazard and risk zoning for land use planning. Eng Geol, 102:85–98.

Fell R, Corominas J, Bonnard C, Cascini L, Leroi E, Savage WZ on behalf of the JTC-1 Joint

Technical Committee on Landslides and Engineered Slopes (2008b) Guidelines for landslide susceptibility, hazard and risk zoning for land-use planning, Commentary. Eng Geol, 102:99–111.

Ferlisi S, Peduto D, Gullà G, Nicodemo G, Borrelli L, Fornaro G (2015) The use of DInSAR data for the analysis of building damage induced by slow-moving landslides. In: Lollino G, Giordan D, Crosta GB, J. Corominas J, Azzam R, Wasowski J, Sciarra N (Eds.), Engineering Geology for Society and Territory – Landslide Processes, © Springer International Publishing – Vol. 2, pp. 1835-1839. doi: 10.1007/978-3-319-09057-3_325.

Ferretti A, Prati C, Rocca F (2001) Permanent scatterers in SAR interferometry. IEEE Transactions on Geoscience and Remote Sensing, 39(1):8-20.

Fornaro G, Lombardini F, Pauciullo A, Reale D, Viviani F (2014) Tomographic Processing of Interferometric SAR Data: Developments, applications, and future research perspectives. IEEE Signal Processing Magazine, 31(4): 41-50.

Fornaro G, Reale D, Serafino F (2009) Four-dimensional SAR imaging for height estimation and monitoring of single and double scatterers. IEEE Trans Geosci Remote Sens, 47(1):224–237.

Fotopoulou SD, Pitilakis KD (2013) Vulnerability assessment of reinforced concrete buildings subjected to seismically triggered slow-moving earth slides. Landslides, 10(5): 563-582, doi:10.1007/s10346-012-0345-5.

Glade T (2003) Vulnerability assessment in landslide risk analysis. Die Erde 134:123–146.

Gullà G, Peduto D, Borrelli L, Antronico L, Fornaro G (2017) Geometric and kinematic characterization of landslides affecting urban areas: the Lungro case study (Calabria, Southern Italy). Landslides, 14: 171-188, doi: 10.1007/s10346-015-0676-0.

Lagomarsino S, Giovinazzi S (2006) Macroseismic and mechanical models for the vulnerability and damage assessment of current buildings. Bull Earthquake Eng, 4(4):415–443.

Leone F, Asté JP, Leroi E (1996) Vulnerability assessment of elements exposed to mass-movement: Working toward a better risk perception. In: Senneset K (Ed.), Landslides, Proc of the 7th Int Symp on Landslides, A.A. Balkema Publishers – Vol. 1, pp. 263–269.

Li Z, Nadim F, Huang H, Uzielli M. Lacasse S (2010) Quantitative vulnerability estimation for scenario-based landslide hazards. Landslides, 7:125–134, doi: 10.1007/s10346-009-0190-3.

Lu P, Catani F, Tofani V, Casagli N (2014) Quantitative hazard and risk assessment for slow-moving landslides from Persistent Scatterer Interferometry. Landslides, 11:685–696, doi: 10.1007/s10346-013-0432-2.

Mansour MF, Morgenstern NR, Martin CD (2011) Expected damage from displacement of slow-moving slides. Landslides, 7:117–131.

This is a post-peer-review, pre-copyedit version of an article published in **LANDSLIDES**. The final authenticated version is available online at: **http://dx.doi.org/10.1007/s10346-017-0826-7**

Maquaire O, Thiery Y, Malet J-P, Weber C, Puissant A, Wania A (2004) Current practices and assessment tools of landslide vulnerability in mountainous basins – identification of exposed elements with a semi-automatic procedure. In: Lacerda W, Ehrlich M, Fontoura SAB, Sayão ASF (Eds.). Landslides: evaluation and stabilization. Proc of the 9th Int Symp on Landslides. A.A. Balkema Publishers – Vol. 1, pp. 171-176.

MATTM (2010) Piano Straordinario di Telerilevamento Ambientale (PSTA), Linee guida per l'analisi dei dati intereferometrici satellitari in aree soggette a dissesti idrogeologici, Italian Ministry of the Environment and Protection of Land and Sea (MATTM), pp. 108.

Mavrouli O, Fotopoulou S, Pitilakis K, Zuccaro G, Corominas J, Santo A, Cacace F, De Gregorio D, Di Crescenzo G, Foerster E, Ulrich T (2014) Vulnerability assessment for reinforced concrete buildings exposed to landslides. Bull Eng Geol Environ, 73:265-289.

Negulescu C, Foerster E (2010) Parametric studies and quantitative assessment of the vulnerability of a RC frame building exposed to differential settlements. Nat Hazards Earth Syst Sci, 10(9):1781-1792.

Negulescu C, Ulrich A, Seyedi DM (2014) Fragility curves for masonry structures submitted to permanent ground displacements and earthquakes. Natural Hazards, 74:1461-1474, doi: 10.1007/s11069-014-1253-x.

Nicodemo G., Peduto D., Ferlisi S., Maccabiani J. (2016) Investigating building settlements via very high resolution SAR sensors. Life-Cycle of Engineering Systems: Emphasis on Sustainable Civil Infrastructure – Bakker, Frangopol & van Breugel (Eds), © 2017 Taylor & Francis Group, London, pp. 2256-2263.

Palmisano F, Vitone C, Cotecchia F, (2016) Landslide damage assessment at the intermediate to small scale. In: Aversa S, Cascini L, Picarelli L, Scavia C (Eds.), Landslides and Engineered Slopes. Experience, Theory and Practice. Proc of the 12th Int Symp on Landslides, CRC Press/Balkema – Vol. 3, pp. 1549-1557.

Peduto D, Borrelli L, Antronico L, Gullà G, Fornaro G (2016a). An integrated approach for landslide characterization in a historic centre. In: Aversa S, Cascini L, Picarelli L, Scavia C (Eds.), Landslides and Engineered Slopes. Experience, Theory and Practice. Proc of the 12th Int Symp on Landslides, CRC Press/Balkema – Vol. 3, 1575-1581.

Peduto D, Cascini L, Arena L, Ferlisi S, Fornaro G, Reale D (2015) A general framework and related procedures for multiscale analyses of DInSAR data in subsiding urban areas. ISPRS Journal of Photogrammetry and Remote Sensing, 105:186-210, doi: 10.1016/j.isprsjprs.2015.04.001.

Peduto D, Huber M, Speranza G, van Ruijven J, Cascini L (2016b). DInSAR data assimilation for settlement prediction: case study of a railway embankment in The Netherlands. Canadian Geotechnical Journal, Published on the web 10 November 2016, doi: 10.1139/cgj-2016-0425.

This is a post-peer-review, pre-copyedit version of an article published in **LANDSLIDES**. The final authenticated version is available online at: **http://dx.doi.org/10.1007/s10346-017-0826-7**

Peduto D, Nicodemo G, Maccabiani J, Ferlisi S (2017) Multi-scale analysis of settlement-induced building damage using damage surveys and DInSAR data: A case study in The Netherlands. Eng Geol, 218: 117–133, doi: 10.1016/j.enggeo.2016.12.018.

Peduto D, Nicodemo G, Maccabiani J, Ferlisi S, D'Angelo R, Marchese A (2016c). Investigating the behaviour of buildings with different foundation types on soft soils: two case studies in The Netherlands. VI Italian Conference of Researchers in Geotechnical Engineering, CNRIG2016 - Geotechnical Engineering in Multidisciplinary Research: from Microscale to Regional Scale, 22-23 September 2016, Bologna (Italy). Procedia Engineering, 158:529–534, http://dx.doi.org/10.1016/j.proeng.2016.08.484.

Peduto D, Pisciotta G, Nicodemo G, Arena L, Ferlisi S, Gullà G, Borrelli L, Fornaro G, Reale D (2016d). A procedure for the analysis of building vulnerability to slow-moving landslides, in: Daponte P, Simonelli AL (Eds.), Proc of the 1st IMEKO TC4 Int Workshop on Metrology for Geotechnics – Benevento, Italy, March 17-18, 2016 – pp. 248-254.

Pisciotta G (2008) Physical vulnerability of elements at risk in landslide prone areas. PhD Thesis, University of Salerno, Italy, pp. 270.

Pitilakis KD, Fotopoulou SD (2015). Vulnerability assessment of buildings exposed to co-seismic permanent slope displacements. In: Winter MG, Smith DM, Eldred PJL, Toll DG (Eds.), Geotechnical Engineering for Infrastructure and Development, ICE Publishing, pp.151-173, doi:10.1680/ecsmge.60678.

Pratesi F, Tapete D, Terenzi G, Del Ventisette C, Moretti S (2015a). Structural Assessment of Case Study Historical and Modern Buildings in the Florentine Area Based on a PSI-Driven Seismic and Hydrogeological Risk Analysis. In: Lollino G, Giordan D, Marunteanu C, Christaras B, Yoshinori I, Margottini C (Eds.), Engineering Geology for Society and Territory Preservation of Cultural Heritage, © Springer International Publishing – Vol. 8, pp. 345-349 . doi: 10.1007/978-3-319-09408-3_60,

Pratesi F, Tapete D, Terenzi G, Del Ventisette C, Moretti S (2015b). Rating health and stability of engineering structures via classification indexes of InSAR Persistent Scatterers. International Journal of Applied Earth Observation and Geoinformation, 40:81–90.

Remondo J, Bonachea J, Cendrero A (2005) A statistical approach to landslide risk modelling at basin scale: from landslide susceptibility to quantitative risk assessment. Landslides, 2:321–328.

Saeidi A, Deck O, Verdel T (2009) Development of building vulnerability functions in subsidence regions from empirical methods. Eng Struct, 31:2275-2286.

Saeidi A, Deck O, Verdel T (2012) Development of building vulnerability functions in subsidence regions from analytical methods. Géotechnique, 62(2):107-120, doi:

10.1680/geot.9.P.028

Sanabria MP, Guardiola-Albert C, Tomas R, Herrera G, Prieto A, Sanchez H, Tessitore S (2014) Subsidence activity maps derived from DInSAR data: Orihuela case study. Natural Hazards and Earth System Sciences 14:1341–1360.

Scavia C, Castelli M (2003) The IMIRILAND project- Impact of Large Landslides in the Mountain Environment: identification and Mitigation of Risk, in: Seismic and Landslide Risk in the European Union, edited by: Yeroyianni, M., Workshop Proceedings, 12–13 November 2002, pp 82–91.

Skempton AW, MacDonald DH (1956). Allowable settlement of buildings. Proc. of the ICE (Institute of Civil Engineers), Pt. III, Vol. 5, pp. 727–768.

United Nations Environment Programme (UNEP) (1997) World Atlas of Desertification. Second Edition, Nairobi, pp. 182 – ISBN: 0340691662.

Uzielli M, Nadim F, Lacasse S, Kaynia AM (2008) A conceptual framework for quantitative estimation of physical vulnerability to landslides. Eng Geol, 102, 3:251-256.

van Westen CJ (2004) Geo-information tools for landslide risk assessment: an overview of recent developments. In: Lacerda W, Ehrlich M, Fontoura SAB, Sayão ASF (Eds.). Landslides: evaluation and stabilization. Proceedings of the 9th Int Symp on Landslides, A.A. Balkema Publishers – Vol. 1, pp. 39-56.

van Westen CJ, Castellanos Abella EA, Sekhar LK (2008) Spatial data for landslide susceptibility, hazards and vulnerability assessment: an overview. Eng Geol, 102, 3-4:112-131.

This is a post-peer-review, pre-copyedit version of an article published in **LANDSLIDES**. The final authenticated version is available online at: **http://dx.doi.org/10.1007/s10346-017-0826-7**

List of Figure captions

Fig. 1. Flowchart of the proposed procedure for the retrieval of fragility/vulnerability curves.

Fig. 2. a) Landslide inventory map of the study area at medium scale; b) spatial distribution of projectable DInSAR data provided by ERS radar sensor on ascending and descending orbit in the period 1992-2000.

Fig. 3. a) Spatial distribution of damaged masonry buildings within landslide-affected areas; b) some examples of damages recorded to buildings, with widespread cracks and extensive damage or tilting, induced by slow-moving landslides.

Fig. 4. a) Example of buildings aggregates characterized by homogeneity of structural (all masonry) and occupancy type; b) an example of vulnerable areas in the municipality of Pesco Sannita (Benevento Province, Campania region).

Fig. 5. a) Percentage distribution of the ED severity level recorded in the vulnerable areas of the study area; b) number of vulnerable areas with a given ED severity level vs. the recognized landslide types; examples of maps of c) ED severity level and d) ECD for vulnerable areas in the municipality of Pesco Sannita (Campania region, southern Italy).

Fig. 6. a) Equivalent damage (ED) severity level vs. equivalent cumulative displacement (ECD) for vulnerable areas of masonry building aggregates over the study area; b) class frequency of occurrence for each EDk (k = 1, 2, 3) suffered by vulnerable areas; c) empirical fragility curves with corresponding median $\left(\overline{ECD_l}\right)$ and standard deviation (β) parameters; d) empirical vulnerability curve.

Figure 7. The study area and the map of typified landslides at large scale (modified from Gullà et al. 2016) and of surveyed buildings distinguished according to the recorded level of damage severity and their distribution based on b) building typology and c) typified landslides. For a detailed description of typified landslide features, the reader can refer to Table II.

Fig. 8. DInSAR data distribution map over the study area at large scale: a) ENVISAT DInSAR benchmarks on ascending orbit for the period 2003-2010 and b) COSMO-SkyMed DInSAR benchmarks on ascending orbit for the period 2012-2014.

Fig. 9. Monitoring of building damage evolution over the time via DInSAR data. The example refers to a reinforced concrete building located on the boundary of an active roto-traslational slide.

Fig. 10. a) Sketch of computation of DInSAR-derived differential settlement (Δ) for each building and b) level of building damage severity (Di, i = 0, ..., 5) collected via fact-sheets during in-situ damage survey. Damage severity level vs. differential settlements for c) reinforced

This is a post-peer-review, pre-copyedit version of an article published in **LANDSLIDES**. The final authenticated version is available online at: **http://dx.doi.org/10.1007/s10346-017-0826-7**

concrete and d) masonry buildings (for the legend of typified landslides, the reader can refer to Table III).

Fig. 11. a) Class frequency of occurrence for each damage level Di (i = 1, ..., 5) suffered by single masonry buildings; b) empirical fragility curves with corresponding median $(\overline{\Delta_l})$ and standard deviation (β) parameters; c) empirical vulnerability curve.

Fig. 12. Results of the K-S goodness-of-fit test of the log-normal distribution function used for the generation of fragility curves for a) vulnerable areas composed by masonry building aggregates in the study area at medium scale and b) single masonry buildings analyzed in the study area at large scale.

This is a post-peer-review, pre-copyedit version of an article published in **LANDSLIDES**. The final authenticated version is available online at: **http://dx.doi.org/10.1007/s10346-017-0826-7**

Table I. Levels of damage severity along with their description (adapted from Burland et al. 1977).

Level of damage severity	Damage description
D0 (Negligible)	Hairline cracks are mainly caused by shrinkage and thermal gradients. Typical widths are less than 0.1 mm
D1 (Very slight)	Cracks are fine and rarely visible; they can be easily treated via normal decoration. Typical crack widths are up to 1 mm.
D2 (Slight)	Visible cracks can be masked by suitable linings or easily filled. Doors and windows might stick slightly. Typical crack widths are up to 5 mm.
D3 (Moderate)	Cracks are much visible; they require some opening up and can be patched by a mason. Doors and windows might stick; whereas service pipes might fracture. Typical crack widths are 5 to 15 mm.
D4 (Severe)	Widespread cracks and extensive damage that requires breaking-out and replacing sections of walls, especially over doors and windows. Settlement might cause slight tilt to walls and onset of fractures to structural elements. Typical cracks widths are 15 to 25 mm, but also the number of cracks is to be taken into account.
D5 (Very severe)	Extensive cracking with structural damage that requires a major repair job involving partial or complete rebuilding. Settlements might cause tilt to walls and instabilities requiring the building evacuation. Typical cracks widths are greater than 25 mm, but also the number of cracks is to be taken into account.

Table II. Main features of the typified landslides in Lungro urban area (modified from Gullà et al. 2016).

Typified landslide	Width (W) [m]	Length (L) [m]	L/W	Depth [m]	Velocity [cm/year]		Involved soil	Kinematic type
					ordinary	critical		
T_A1	25-100	≤ 180	≤ 2.5	about 6	2-4	> 200	detritic-colluvial covers	Complex landslide
T_A2	15-100	≥ 80	> 2.5	about 10	5-7	> 20		
T_B1	90-260	130-550	< 2.5	10-20	0.5-5	> 80	deeply weathered and chaotic phyllites	Complex landslide
T_B2	80-220	>300	≥ 2.5	10-16	4-20	> 100		
T_C	830	1500	1.8	20-30	0.5-5	> 40	deeply weathered and chaotic phyllites	Landslide zone
T_D	100-250	350-550	2.2-3.2	20-30 /10-15	0.2-0.5	2-5	weathered and chaotic phyllites	Slide

Figure_1

Click here to download Figure Fig. 1.tif

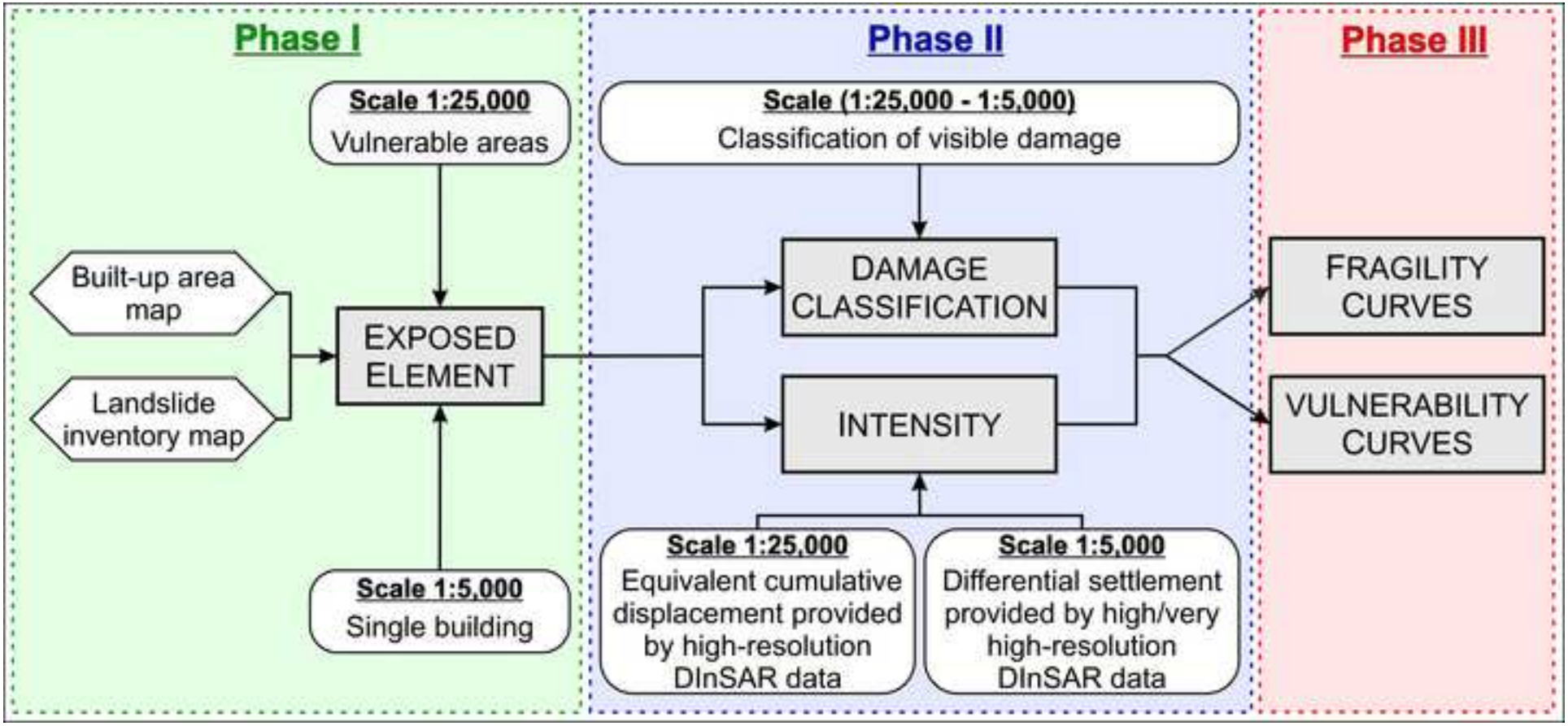

Figure_2

Click here to download Figure Fig. 2.tif

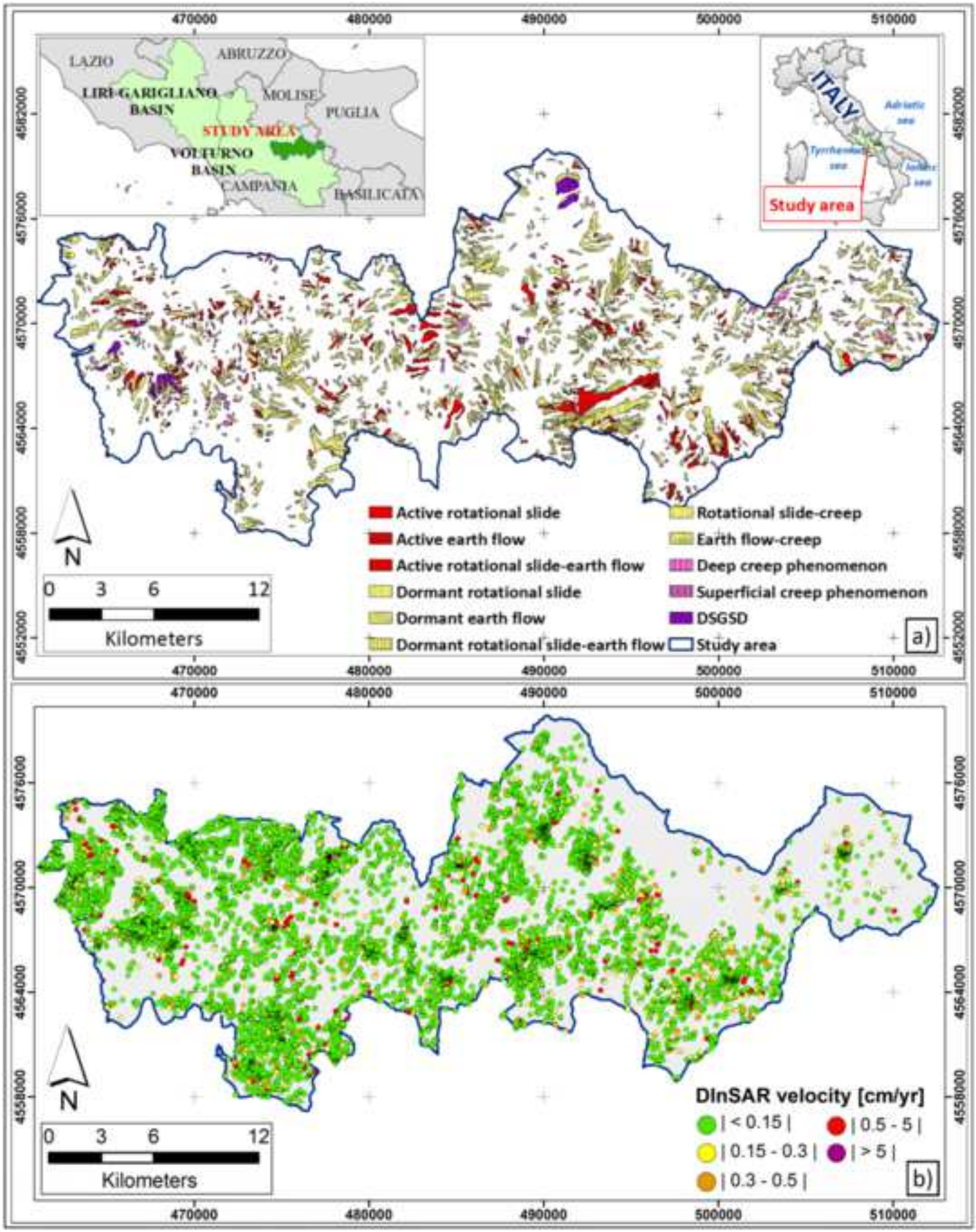

Figure_3

Click here to download Figure Fig. 3.tif

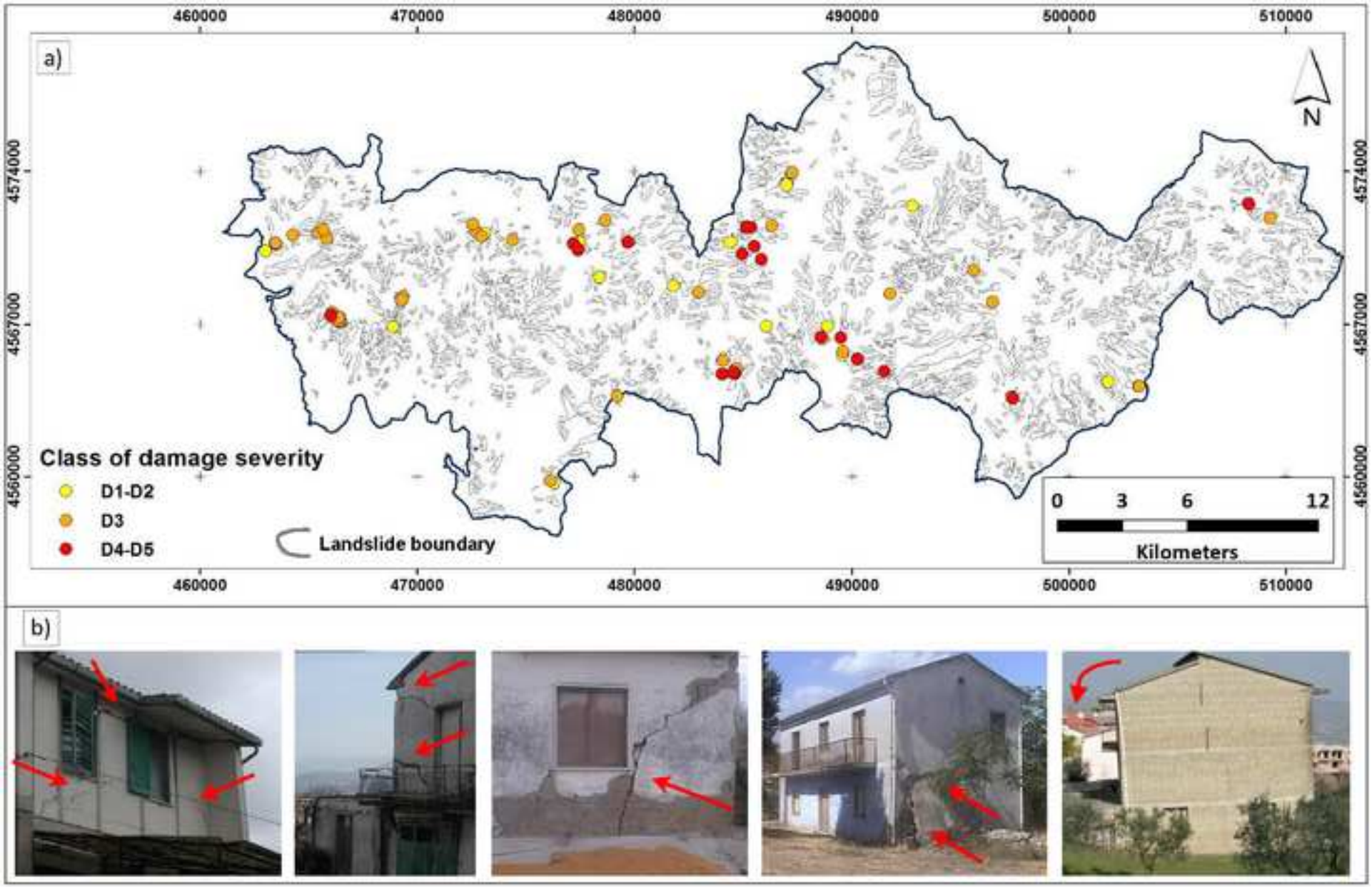

Figure_4

Click here to download Figure Fig. 4.tif

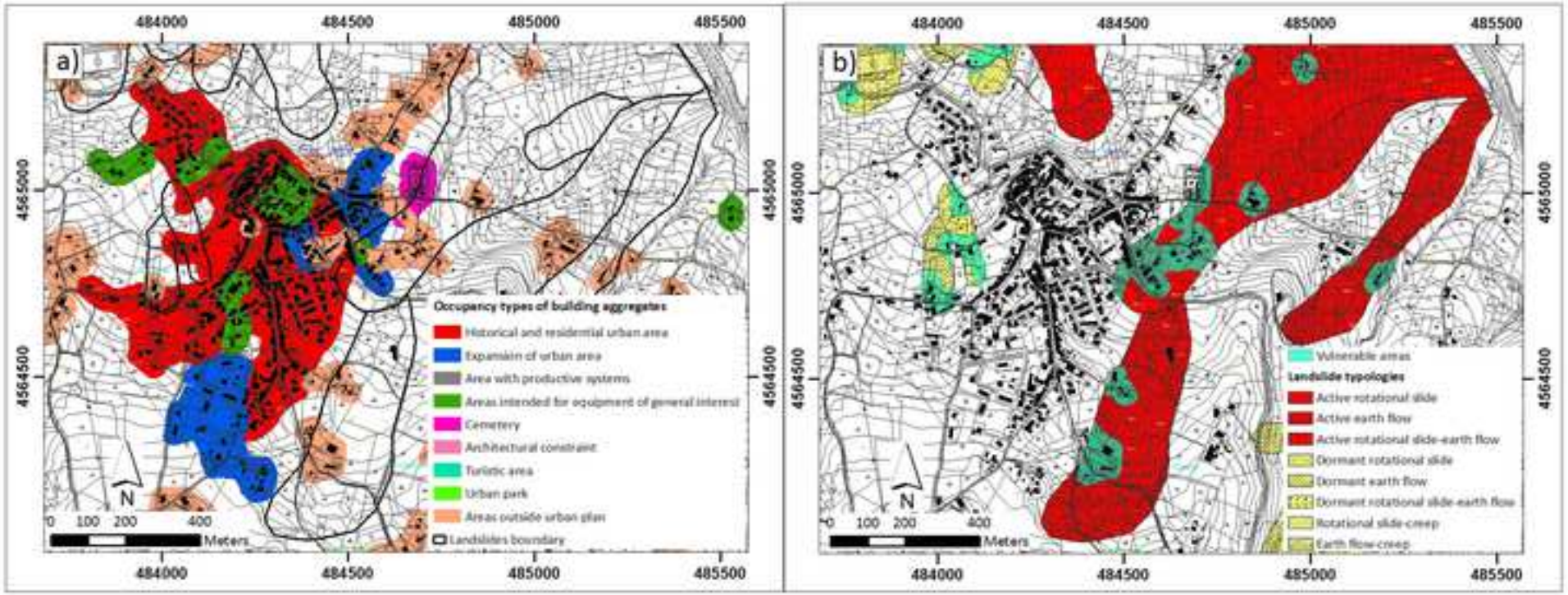

Figure_5

Click here to download Figure Fig. 5.tif

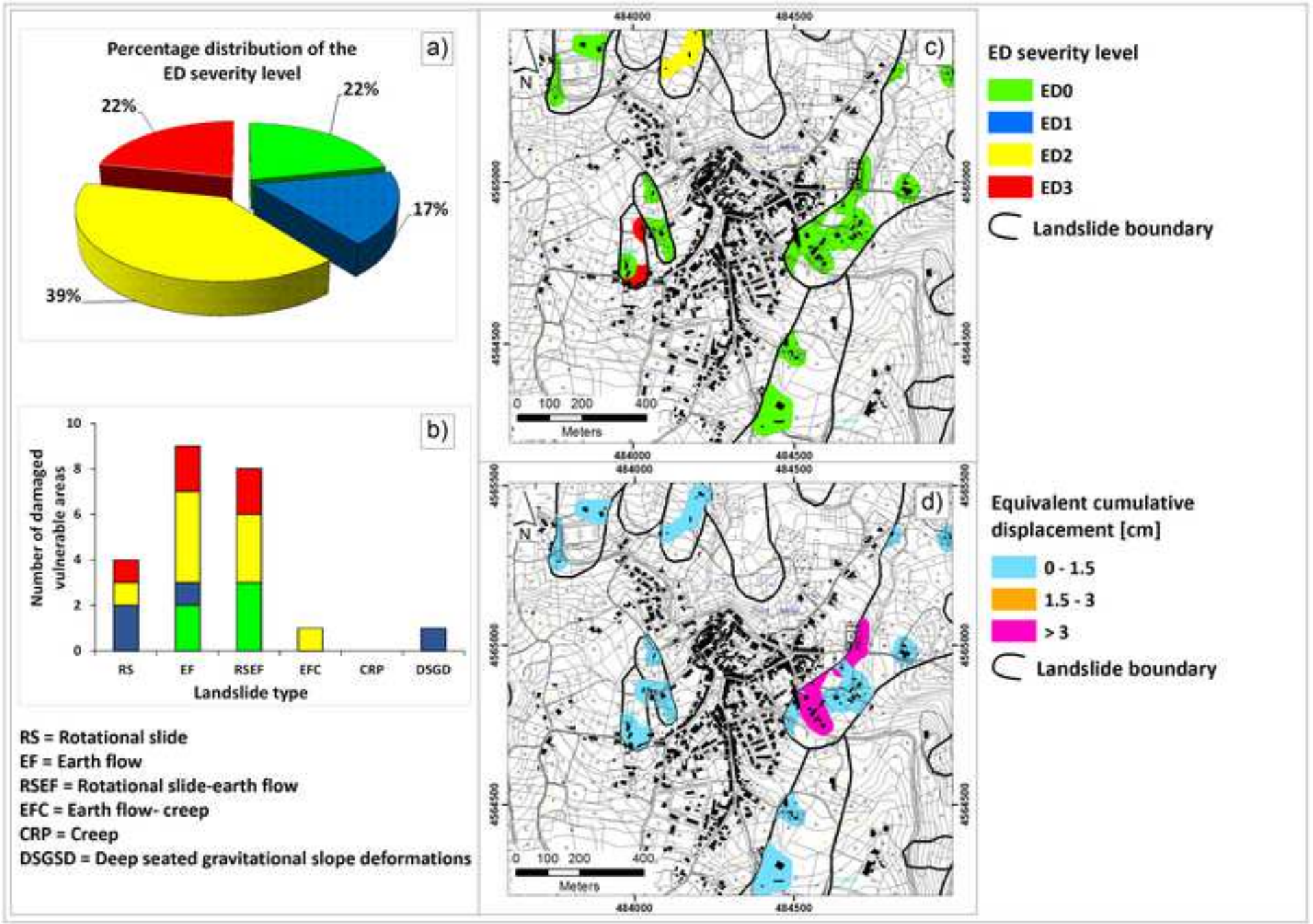

Figure_6

Click here to download Figure Fig. 6.tif

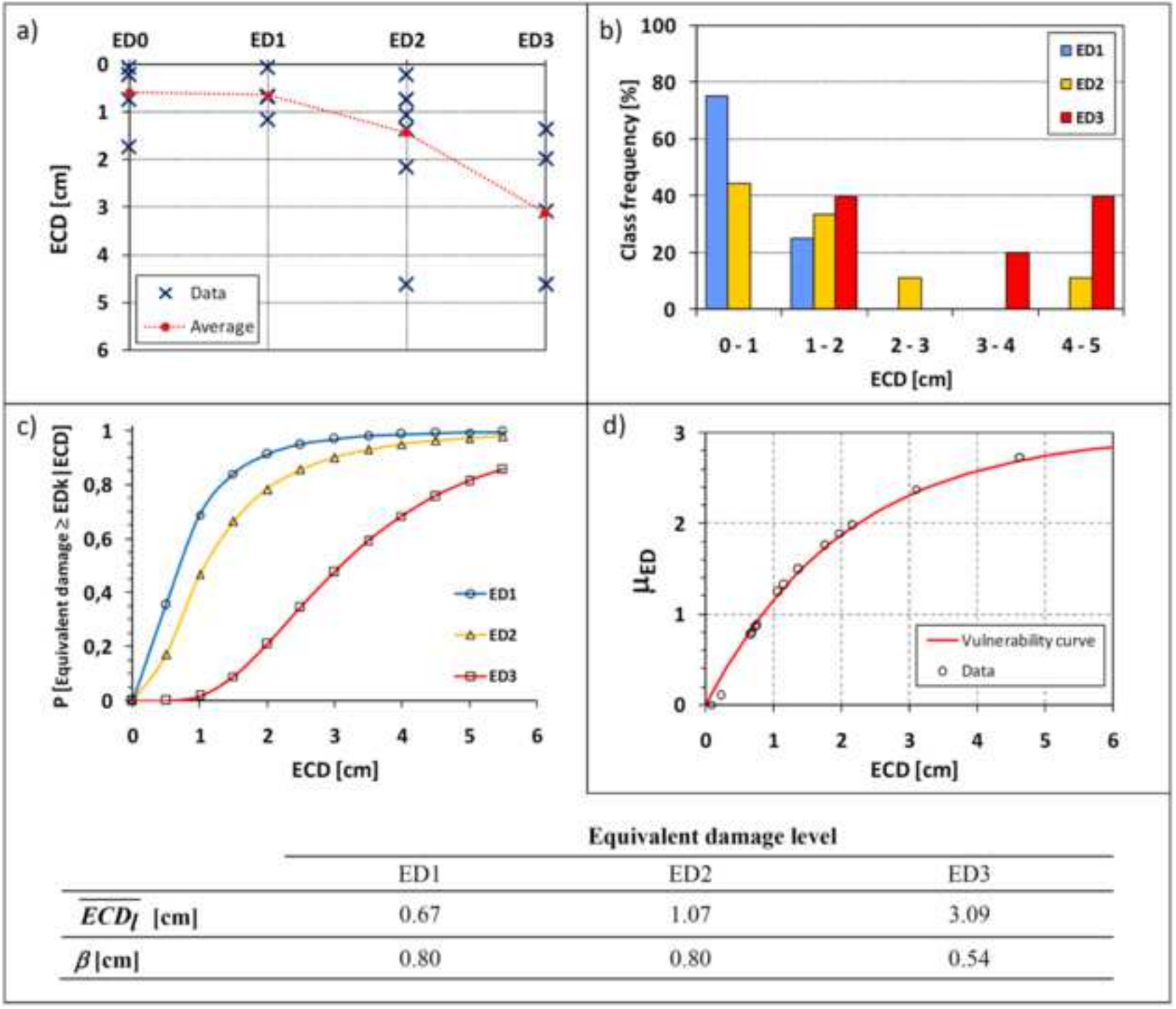

	Equivalent damage level		
	ED1	ED2	ED3
$\overline{ECD_f}$ [cm]	0.67	1.07	3.09
β [cm]	0.80	0.80	0.54

Figure_7

Click here to download Figure Fig. 7.tif

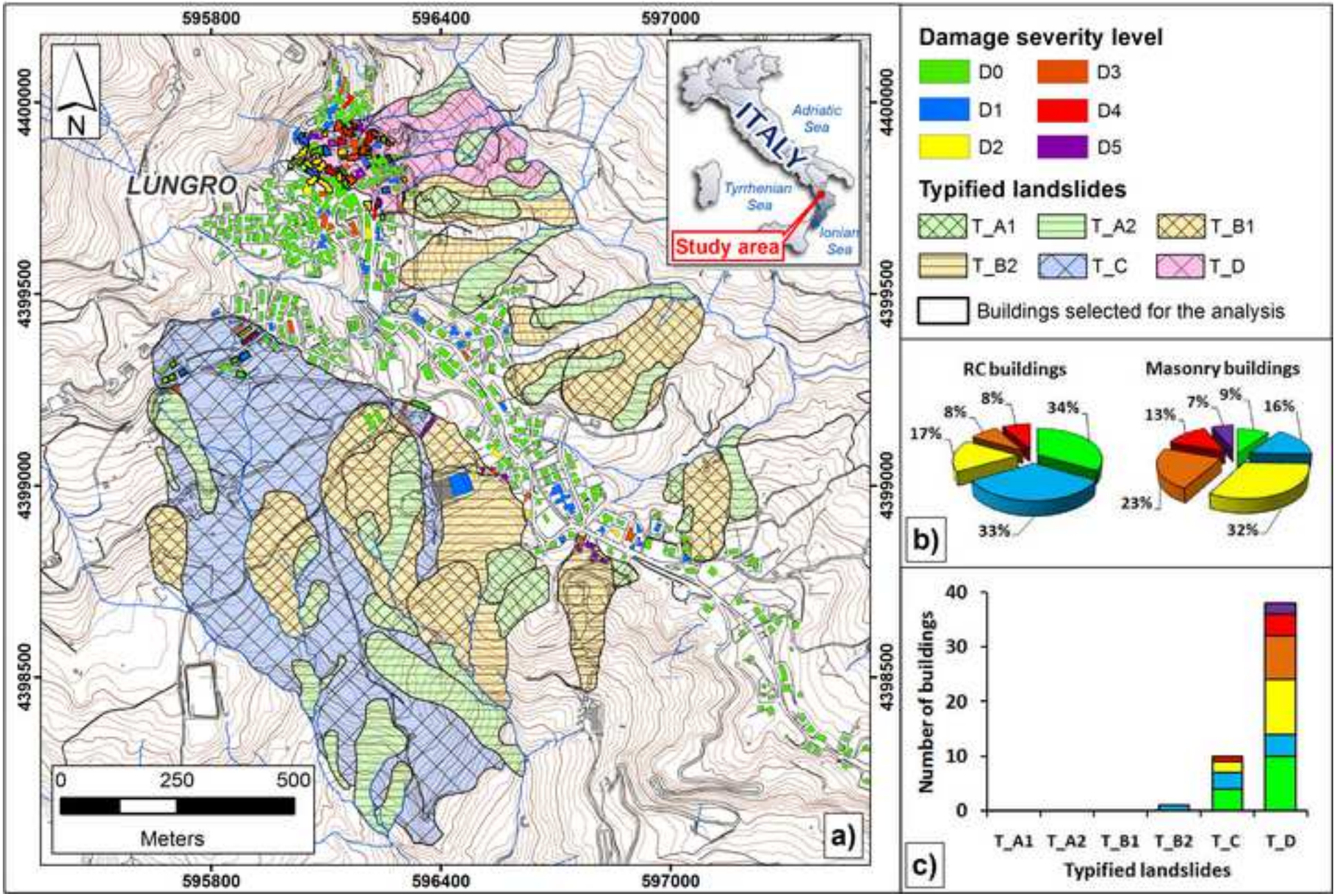

Figure_8

Click here to download Figure Fig. 8.tif

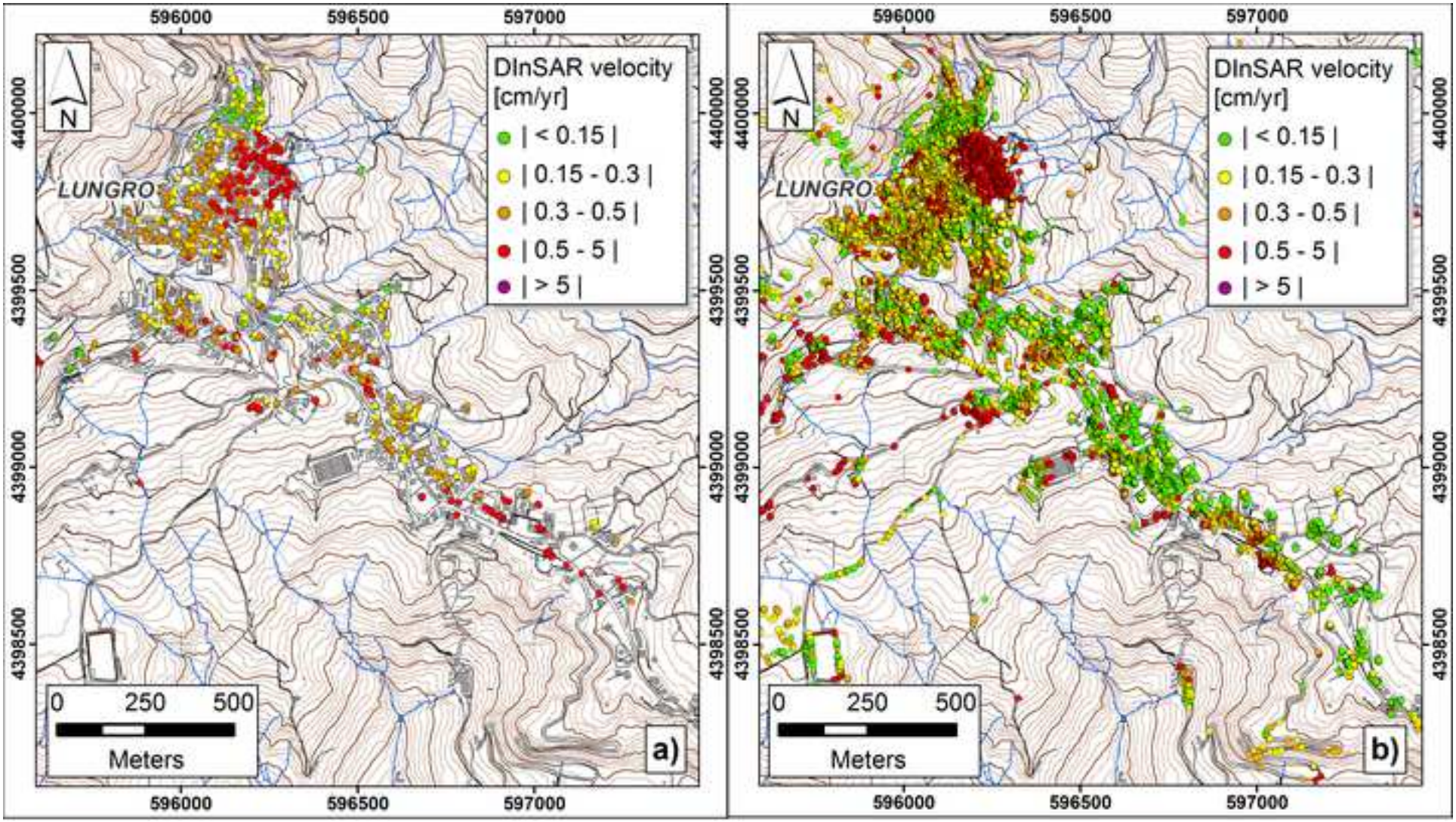

Figure_9

Click here to download Figure Fig. 9.tif

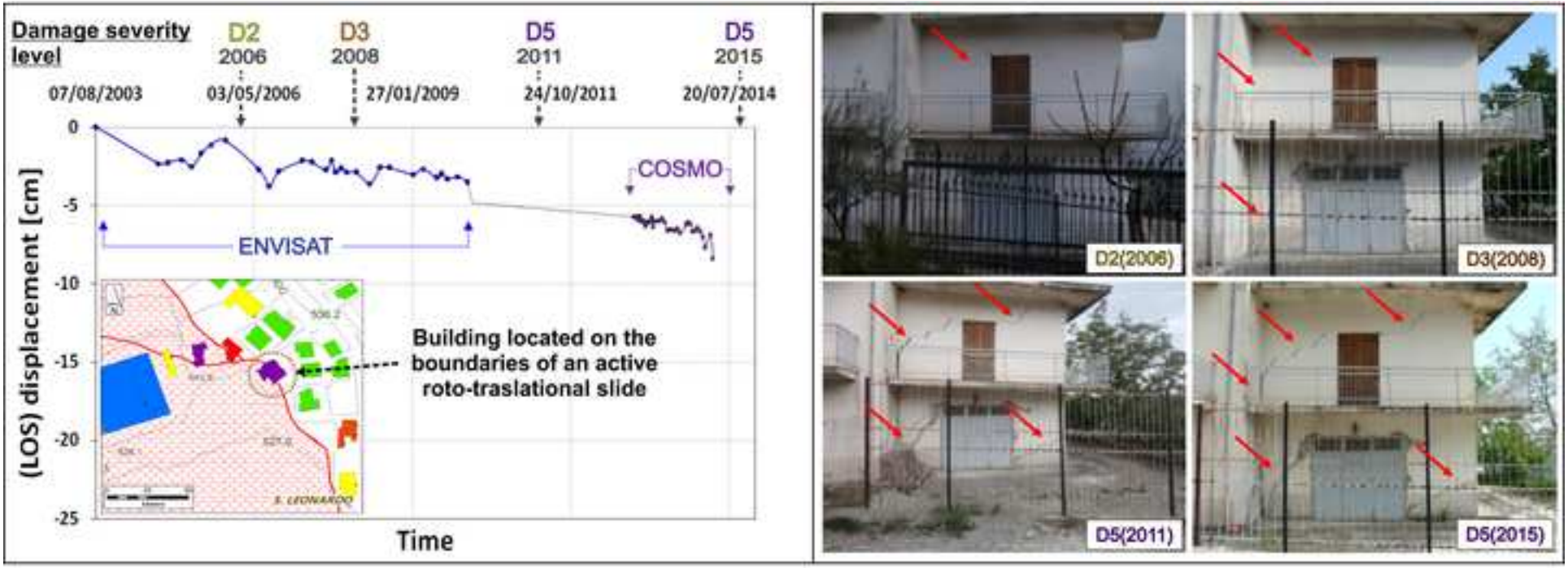

Figure_10

Click here to download Figure Fig. 10.tif

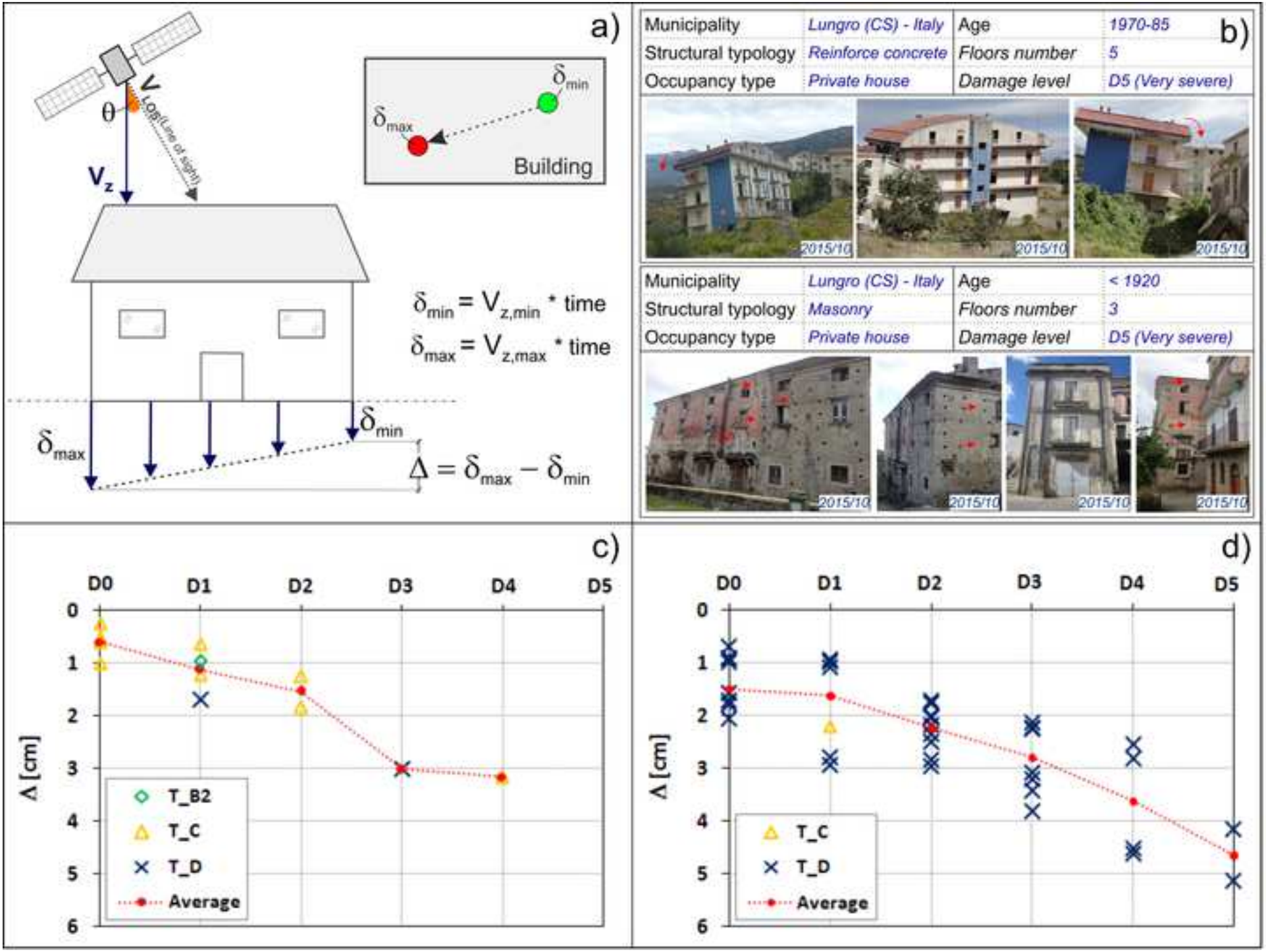

Figure_11

Click here to download Figure Fig. 11.tif

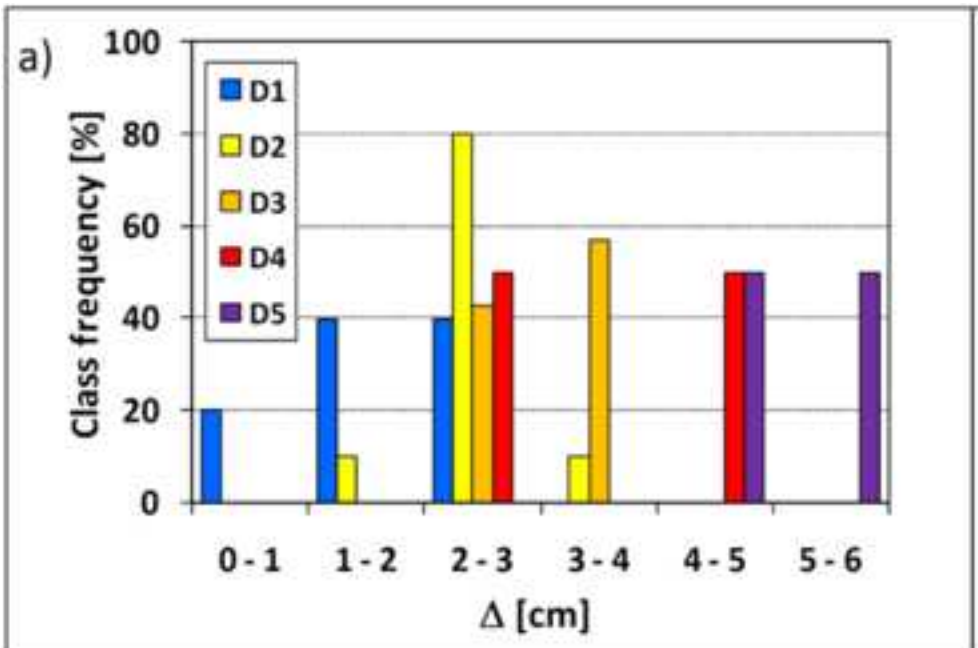

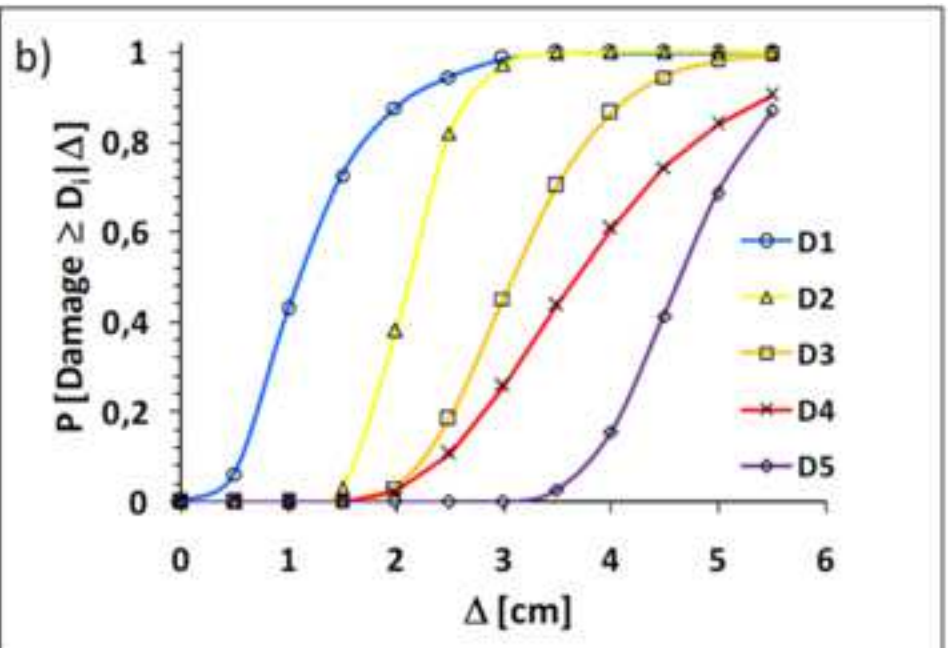

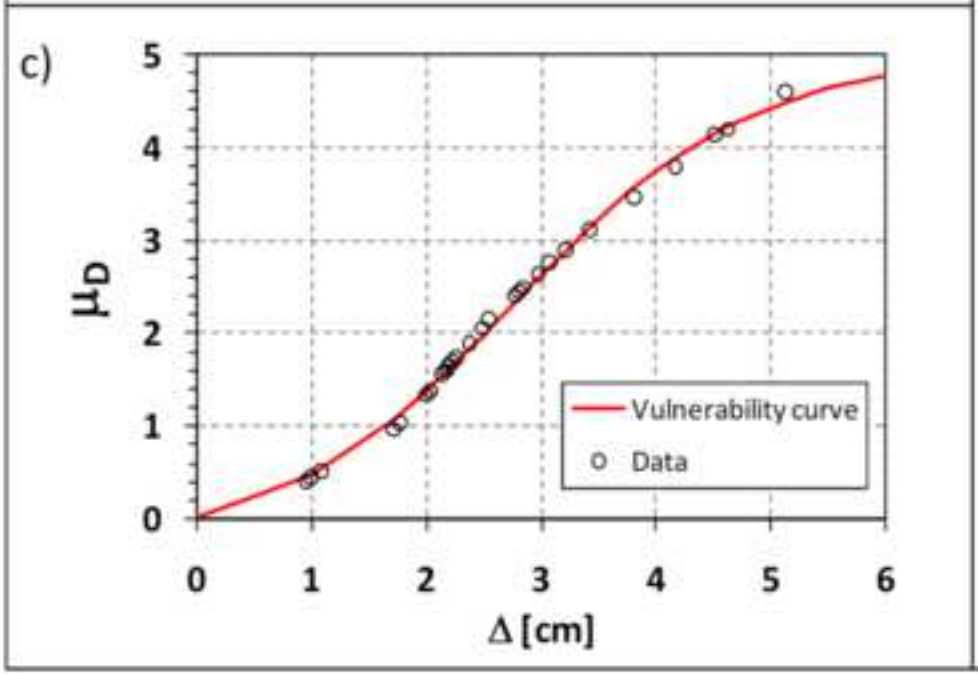

Damage severity level	$\overline{\Delta_i}$ [cm]	β [cm]
D1 (very slight)	1,10	0.50
D2 (slight)	2,11	0.18
D3 (moderate)	3,08	0.24
D4 (severe)	3,67	0.31
D5 (very severe)	4,65	0.15

Figure_12

Click here to download Figure Fig. 12.tif

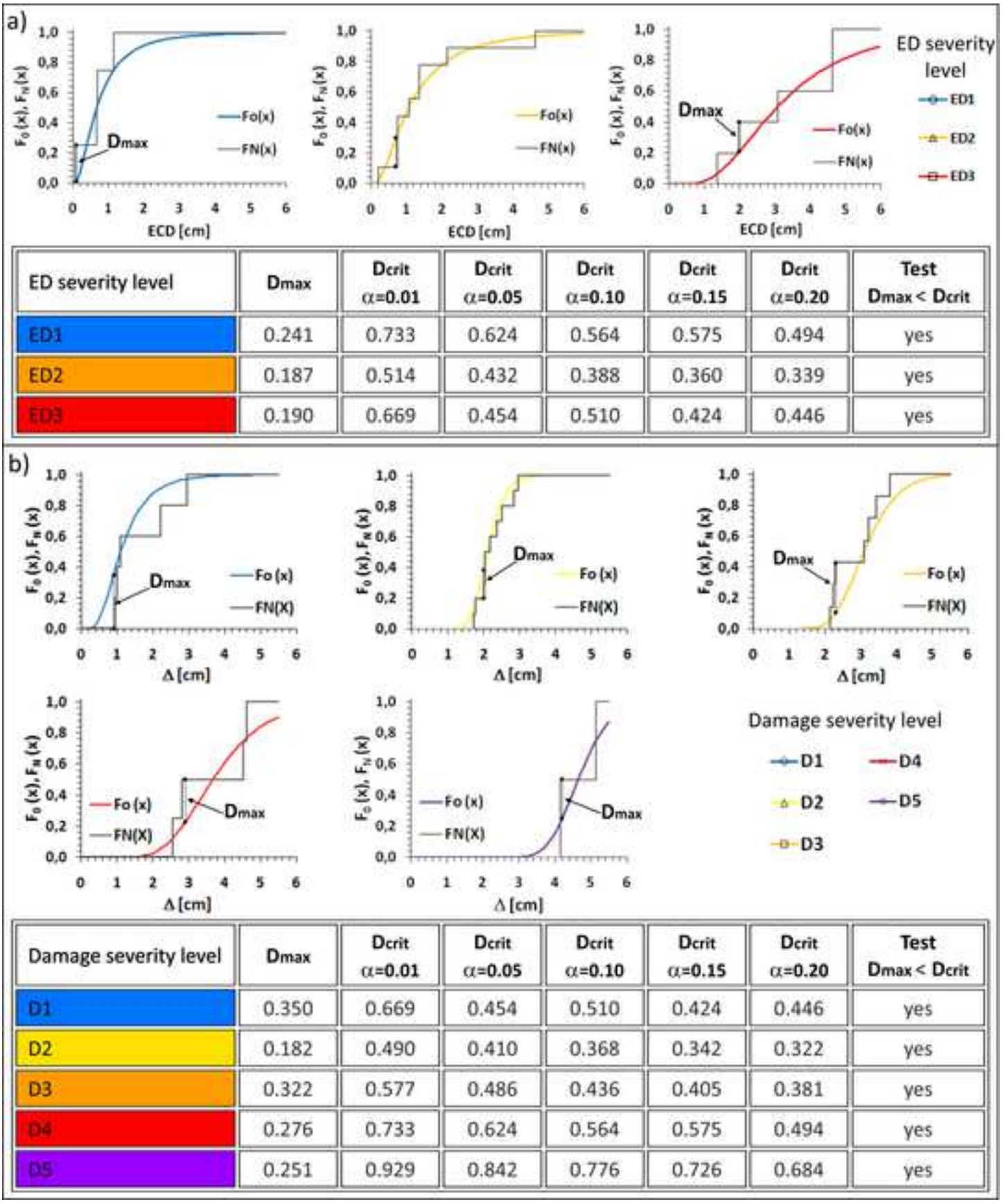

ED severity level	Dmax	Dcrit α=0.01	Dcrit α=0.05	Dcrit α=0.10	Dcrit α=0.15	Dcrit α=0.20	Test Dmax < Dcrit
ED1	0.241	0.733	0.624	0.564	0.575	0.494	yes
ED2	0.187	0.514	0.432	0.388	0.360	0.339	yes
ED3	0.190	0.669	0.454	0.510	0.424	0.446	yes

Damage severity level	Dmax	Dcrit α=0.01	Dcrit α=0.05	Dcrit α=0.10	Dcrit α=0.15	Dcrit α=0.20	Test Dmax < Dcrit
D1	0.350	0.669	0.454	0.510	0.424	0.446	yes
D2	0.182	0.490	0.410	0.368	0.342	0.322	yes
D3	0.322	0.577	0.486	0.436	0.405	0.381	yes
D4	0.276	0.733	0.624	0.564	0.575	0.494	yes
D5	0.251	0.929	0.842	0.776	0.726	0.684	yes